



Calhoun: The NPS Institutional Archive
DSpace Repository

NPS Scholarship

Theses

2008-12

High bandwidth communications links
between heterogeneous autonomous vehicles
using sensor network modeling and
extremum control approaches

Kam, Khim Yee.

Monterey, California. Naval Postgraduate School

<https://hdl.handle.net/10945/3833>

Downloaded from NPS Archive: Calhoun



Calhoun is the Naval Postgraduate School's public access digital repository for research materials and institutional publications created by the NPS community. Calhoun is named for Professor of Mathematics Guy K. Calhoun, NPS's first appointed -- and published -- scholarly author.

Dudley Knox Library / Naval Postgraduate School
411 Dyer Road / 1 University Circle
Monterey, California USA 93943

<http://www.nps.edu/library>



**NAVAL
POSTGRADUATE
SCHOOL**

MONTEREY, CALIFORNIA

THESIS

**HIGH BANDWIDTH COMMUNICATIONS LINKS
BETWEEN HETEROGENEOUS AUTONOMOUS
VEHICLES USING SENSOR NETWORK MODELING AND
EXTREMUM CONTROL APPROACHES**

by

Khim Yee Kam

December 2008

Thesis Co-Advisors:

Isaac I. Kaminer

Deok Jin Lee

Approved for public release; distribution is unlimited

THIS PAGE INTENTIONALLY LEFT BLANK

REPORT DOCUMENTATION PAGE			<i>Form Approved OMB No. 0704-0188</i>	
Public reporting burden for this collection of information is estimated to average 1 hour per response, including the time for reviewing instruction, searching existing data sources, gathering and maintaining the data needed, and completing and reviewing the collection of information. Send comments regarding this burden estimate or any other aspect of this collection of information, including suggestions for reducing this burden, to Washington headquarters Services, Directorate for Information Operations and Reports, 1215 Jefferson Davis Highway, Suite 1204, Arlington, VA 22202-4302, and to the Office of Management and Budget, Paperwork Reduction Project (0704-0188) Washington DC 20503.				
1. AGENCY USE ONLY (Leave blank)		2. REPORT DATE December 2008	3. REPORT TYPE AND DATES COVERED Master's Thesis	
4. TITLE AND SUBTITLE High Bandwidth Communications Links Between Heterogeneous Autonomous Vehicles Using Sensor Network Modeling and Extremum Control Approaches			5. FUNDING NUMBERS	
6. AUTHOR(S) Kam Khim Yee				
7. PERFORMING ORGANIZATION NAME(S) AND ADDRESS(ES) Naval Postgraduate School Monterey, CA 93943-5000			8. PERFORMING ORGANIZATION REPORT NUMBER	
9. SPONSORING /MONITORING AGENCY NAME(S) AND ADDRESS(ES) N/A			10. SPONSORING/MONITORING AGENCY REPORT NUMBER	
11. SUPPLEMENTARY NOTES The views expressed in this thesis are those of the author and do not reflect the official policy or position of the Department of Defense or the U.S. Government.				
12a. DISTRIBUTION / AVAILABILITY STATEMENT Approved for public release; distribution is unlimited			12b. DISTRIBUTION CODE	
13. ABSTRACT (maximum 200 words) <p>In future network-centric warfare environments, teams of autonomous vehicles will be deployed in a cooperative manner to conduct wide-area intelligence, surveillance and reconnaissance (ISR) missions in a tactical environment. The operational range of these survey vehicles is usually limited by the line-of-sight (LOS) and/or bandwidth constraints of the communication system. To increase the operational range and to allow real-time transmission of data back to the command station, autonomous vehicles configured with high bandwidth communication system are positioned between the command station and the survey vehicles acting as communication relay vehicles and flying sensors. This will allow the survey vehicles to transfer their data back to the command station on the move, thus improving the efficiency of the missions.</p> <p>In this thesis, an autopilot guidance and control algorithm was developed that will allow the relay vehicles to reposition themselves autonomously to maintain an optimal loitering flight path to maximize the quality of the communication link between the command station and survey vehicle. The main contributions of this thesis are two-fold. First, a communication propagation model was developed to predict the signal-to-noise (SNR) ratio of the communication link, which is used as a reference SNR signal for the UAVs. Second, the communication model was then integrated into a feedback control loop to formulate a new real-time adaptive controller, which is based on an extremum seeking approach with a gradient-based controller, to drive the relay vehicle to an optimal loitering path using SNR as the cost function.</p>				
14. SUBJECT TERMS Unmanned Aerial Vehicle, UAV, Extremum Seeking, Simulink, High Bandwidth Communication Links, SNR Model			15. NUMBER OF PAGES 75	
			16. PRICE CODE	
17. SECURITY CLASSIFICATION OF REPORT Unclassified	18. SECURITY CLASSIFICATION OF THIS PAGE Unclassified	19. SECURITY CLASSIFICATION OF ABSTRACT Unclassified	20. LIMITATION OF ABSTRACT UU	

THIS PAGE INTENTIONALLY LEFT BLANK

Approved for public release; distribution in unlimited

**HIGH BANDWIDTH COMMUNICATIONS LINKS BETWEEN
HETEROGENEOUS AUTONOMOUS VEHICLES USING SENSOR NETWORK
MODELING AND EXTREMUM CONTROL APPROACHES**

Khim Yee Kam
Civilian, Defence Science & Technology Agency
B.Eng (Electrical Engineering), National University of Singapore, 1999

Submitted in partial fulfillment of the
requirements for the degree of

**MASTER OF SCIENCE IN ENGINEERING SCIENCE
(MECHANICAL ENGINEERING)**

from the

**NAVAL POSTGRADUATE SCHOOL
December 2008**

Author: Khim Yee Kam

Approved by: Professor Isaac I. Kaminer
Thesis Co-Advisor

Dr Deok Jin Lee
Thesis Co-Advisor

Professor Knox T. Millsaps
Chairman, Department of Mechanical and Astronautical
Engineering

THIS PAGE INTENTIONALLY LEFT BLANK

ABSTRACT

In future network-centric warfare environments, teams of autonomous vehicles will be deployed in a cooperative manner to conduct wide-area intelligence, surveillance and reconnaissance (ISR) missions in a tactical environment. The operational range of these survey vehicles is usually limited by the line-of-sight (LOS) and/or bandwidth constraints of the communication system. To increase the operational range and to allow real-time transmission of data back to the command station, autonomous vehicles configured with high bandwidth communication system are positioned between the command station and the survey vehicles acting as communication relay vehicles and flying sensors. This will allow the survey vehicles to transfer their data back to the command station on the move, thus improving the efficiency of the missions.

In this thesis, an autopilot guidance and control algorithm was developed that will allow the relay vehicles to reposition themselves autonomously to maintain an optimal loitering flight path to maximize the quality of the communication link between the command station and survey vehicle. The main contributions of this thesis are two-fold. First, a communication propagation model was developed to predict the signal-to-noise (SNR) ratio of the communication link, which is used as a reference SNR signal for the UAVs. Second, the communication model was then integrated into a feedback control loop to formulate a new real-time adaptive controller, which is based on an extremum seeking approach with a gradient-based controller, to drive the relay vehicle to an optimal loitering path using SNR as the cost function.

THIS PAGE INTENTIONALLY LEFT BLANK

TABLE OF CONTENTS

I.	INTRODUCTION.....	1
	A. MOTIVATION	1
	B. TACTICAL NETWORK TOPOLOGY (TNT) PROGRAM.....	1
	C. THESIS OBJECTIVES.....	2
II.	LITERATURE REVIEW	3
	A. CONTROL FOR HIGH BANDWIDTH COMMUNICATIONS LINK ...	3
	1. Introduction to Extremum Seeking Control	3
	2. Extremum Seeking – How Does it Work?	4
	B. AUTONOMOUS VEHICLE COMMUNICATIONS NETWORKS.....	5
	1. Propagation Mechanisms	6
	a. <i>Friis Free Space Equation.....</i>	<i>7</i>
	b. <i>Antenna Gain Patterns</i>	<i>7</i>
	c. <i>Reflection.....</i>	<i>9</i>
	d. <i>Diffraction</i>	<i>9</i>
	e. <i>Scattering.....</i>	<i>9</i>
	2. Propagation Models.....	10
	C. PROPOSED THEORETICAL PROPAGATION MODEL.....	10
III.	FLIGHT CONTROL SYSTEMS	13
	A. SIG RASCAL 110 AIRPLANE	13
	B. WAVE RELAY WIRELESS MESH NETWORK	14
IV.	MODELLING	15
	A. SNR MODEL (MULTI-NODES)	15
	1. UAV Dynamic Model.....	15
	2. LOS Path Loss Model.....	17
	3. Antenna Pattern Loss Model	18
	4. Link Budget Model	20
	B. RASCAL SNR MODEL	21
	C. SNR MAP	22
V.	SNR MODEL VERIFICATION FLIGHT TEST.....	25
	A. BACKGROUND	25
	B. SET-UP	25
	C. FLIGHT TEST RESULTS AND ANALYSIS.....	27
	1. SNR Variation with Distance.....	27
	2. SNR Variation with Altitude.....	28
	3. SNR Variation with GCS Antenna Pattern.....	30
	4. Comparison of Actual Flight Test Data with Mathematical SNR Model.....	31
	5. Comparison of Actual Flight Test Data with SNR Map	34
VI.	EXTREMUM SEEKING CONTROL.....	37
	A. BACKGROUND	37

B.	HARDWARE-IN-THE-LOOP (HIL) TEST	37
1.	HIL Test Set-up.....	38
2.	HIL Test Results	39
VII.	COMMUNICATION LINKS FLIGHT TEST	43
A.	BACKGROUND	43
B.	SNR DATA ACQUISITION & MANAGEMENT	43
C.	SETUP.....	44
D.	FLIGHT TEST RESULTS AND ANALYSIS.....	46
1.	UAV Flight Trajectory	46
2.	SNR Variation along Flight Trajectory	47
3.	Comparison of Actual SNR data with Simulated SNR Data	48
VIII.	CONCLUSIONS & FUTURE WORKS.....	51
A.	CONCLUSIONS	51
B.	FUTURE WORK.....	51
	APPENDIX A. ANTENNA DATASHEETS.....	53
	LIST OF REFERENCES.....	57
	INITIAL DISTRIBUTION LIST	59

LIST OF FIGURES

Figure 1.	Perturbation-based Extremum Seeking Architecture [From Ref. [5]].....	5
Figure 2.	Antenna Pattern for Vertical Polarized Sector Antennas from Laird Technologies (Model SA24-120-9).....	8
Figure 3.	Rascal Unmanned Aerial Vehicle (UAV).....	13
Figure 4.	Wave Relay QAUD Radio Router [From [9]].....	14
Figure 5.	SNR (Multi-Nodes) Model.	16
Figure 6.	UAV Dynamic Model.....	17
Figure 7.	Path Loss Model.	18
Figure 8.	Antenna Pattern Loss Model.....	18
Figure 9.	UAV Bank Angle Effect on the Arrival Angle.....	19
Figure 10.	Geometry Showing the Definition of Bearing, φ	19
Figure 11.	Link Budget Model.....	20
Figure 12.	RASCAL SNR Model.....	23
Figure 13.	SNR Map (X-Y View).....	24
Figure 14.	SNR Map (X-Z View).	24
Figure 15.	Location of GCS and Rascal Flight Paths during Flight Test [From Google Earth].....	26
Figure 16.	Actual SNR Readings along the Rascal Flight Trajectory (3D map) Obtained during Flight Test.....	27
Figure 17.	Actual SNR Readings along the Rascal Flight Trajectory (2D map in east-north) Obtained during Flight Test.	28
Figure 18.	Variations of SNR Readings with Altitude at Paths B and C of the Flight Trajectory.....	29
Figure 19.	Variations of SNR Readings with the GCS Antenna Pattern of the Flight Trajectory.....	30
Figure 20.	Simulated SNR Readings along the Rascal Flight Trajectory (3D map) obtained from Mathematical SNR Model.....	31
Figure 21.	Simulated SNR Readings along the Rascal Flight Trajectory (2D map) obtained from Mathematical SNR Model.....	32
Figure 22.	SNR Error (in %) between Simulated Reading and Actual Flight Data.....	33
Figure 23.	SNR Error (in %) Plotted Against Time.	33
Figure 24.	Actual SNR Data Superimposed onto the SNR Map (East-North View).....	34
Figure 25.	Actual SNR Data Superimposed onto the SNR Map (North View).....	35
Figure 26.	Actual SNR Data Superimposed onto the SNR Map (East View).	35
Figure 27.	Diagram of Extremum Seeking-based Control Strategy for Autonomous UAV Control [From [10]].....	37
Figure 28.	3D Map of SNR Distribution from Two Antenna Nodes [From [10]]	38
Figure 29.	UAV Flight Trajectory with Respect to Two Antenna Nodes Based on Commands from Extremum Seeking Controller [From [10]]	39
Figure 30.	UAV Flight Trajectory Superimposed onto the 2D Projection of the SNR Distribution [From [10]]	40
Figure 31.	SNR Variation with Time between the UAV and Node 1 [From [10]].....	41

Figure 32.	SNR Variation with Time between the UAV and Node 2 [From [10]].....	41
Figure 33.	Rate of Change of the Cost Function (SNR) with Time [From [10]].....	42
Figure 34.	SNR Data Acquisition & Management Structure.....	44
Figure 35.	Relative Location of the GCS node and Remote Node [From Google Earth].....	45
Figure 36.	UAV Flight Path during the TNT Experimental Program.....	46
Figure 37.	SNR Variation with Time between the UAV (sender) and GCS Node (receiver).....	47
Figure 38.	SNR Variation with Time between the Remote Node (sender) and UAV (receiver).....	48
Figure 39.	Actual (Measured) Average SNR (dB) along Rascal Flight Trajectory obtained from Flight Test.....	49
Figure 40.	Simulated Average SNR (dB) along Rascal Flight Trajectory obtained from Flight Test.	49
Figure 41.	SNR Error (in %) between Simulated Reading and Actual Flight Test Data.	50
Figure 42.	Biological Soaring Gliders (NPS).....	52

LIST OF TABLES

Table 1.	Flight Paths of Rascal UAV during Flight Test.....	26
----------	--	----

THIS PAGE INTENTIONALLY LEFT BLANK

ACKNOWLEDGMENTS

First and Foremost, I would like to thank my thesis advisor, Professor Isaac Kaminer for providing me the opportunity to work on this interesting project and for all his guidance throughout the project.

Secondly, I would like to thank my co-advisor, Dr Deok Jin Lee for all his valuable guidance, support and time spent helping me in this project. When I need help, Dr Lee has been most willingly to offer his professional advice and guidance. I would also like to thank Professor Kevin Jones and Dr Song Kwang for all the support they provided during the project.

Lastly, I want to express my gratitude to my wife and daughter for their understanding and continued support during the course of my studies at Naval Postgraduate School.

THIS PAGE INTENTIONALLY LEFT BLANK

I. INTRODUCTION

A. MOTIVATION

In future network-centric warfare environments, teams of autonomous vehicles will be deployed in a cooperative manner to conduct wide-area intelligence, surveillance, and reconnaissance (ISR) missions. When operating in a tactical environment without satellite communications, the operational range of these survey vehicles is usually limited by the line-of-sight (LOS) and/or bandwidth constraints of the communication system. The operational range can be extended if there are other autonomous vehicles positioned between the command station and the survey vehicle, acting as relay vehicles capable of high bandwidth transmission to the command station. This is particularly useful in applications where the survey vehicles are underwater and/or surface vehicles and their range extended by an unmanned aerial vehicle (UAV) relay node orbiting overhead.

The data gathered from the survey vehicles is usually of high priority and time critical. It is critical that these data is transferred in real-time back to the command station for processing into actionable information for decision makers. Relay vehicles configured with high bandwidth transmission will allow survey vehicles to transfer their data while on the move, thus improving the efficiency of the missions.

Researchers at the Unmanned Systems Lab of the Naval Postgraduate School (NPS) are developing autopilot guidance and control algorithms that will allow the relay vehicles to reposition themselves autonomously to maintain an optimal loitering flight path to maximize the quality of the communication link between the command station and survey vehicles [1].

B. TACTICAL NETWORK TOPOLOGY (TNT) PROGRAM

The current research is supported in part by the TNT Cooperative Field Experimentation Program, a joint program between the United States Special Operations Command (USSOCOM), its component commands, and several government laboratories,

including the Unmanned Systems Lab at NPS. The program focuses on the exploration and demonstration of new technologies applicable to the military with special focus in the area of autonomous vehicle and target identification/tracking. Flight tests are conducted quarterly at the Center of Interdisciplinary Remotely-Piloted Aircraft Studies (CIRPAS) facility located at McMillan Air Field in Camp Roberts, California.

C. THESIS OBJECTIVES

There are two objectives to this thesis. The first objective is to develop a propagation model capable of predicting the quality of the communication link. This propagation model is to be used to analyze the variation of free-space propagation loss, antenna pattern loss, and the effect of bank angle on the signal-to-noise ratio (SNR) of the communication link. The second objective is to use the propagation model to develop a new real-time adaptive controller, by means of extremum seeking techniques, to drive the UAV to an optimal loitering flight path using SNR as the cost function.

II. LITERATURE REVIEW

A. CONTROL FOR HIGH BANDWIDTH COMMUNICATIONS LINK

Numerous optimization control techniques are available to control a UAV to maintain an optimal loitering flight path and maximize the communication link quality between the command station and the survey vehicle.

In [2], the author uses an attraction to weaker SNR values and the relative geographical position of the ground nodes to re-position the relay node. The relay node measures the SNR between itself and other subsystems and reacts by moving towards the subsystem with a lower SNR value. Without knowledge of the environment or an accurate propagation model, the use of relative geographical positions alone to control the UAV to an optimal loitering flight path, may not be the right approach. The transmission path between the transmitter and the receiver can vary from a simple line-of-sight (LOS) path to a highly unpredictable path that can not be easily modeled.

An alternative is to use the extremum seeking control technique (see below). In [3], the authors used a Lyapunov guidance vector field (LGVF) controller based on extremum seeking methods to form an optimal communication chain of unmanned aircraft.

1. Introduction to Extremum Seeking Control

Extremum seeking control is an extension of classical adaptive control technique. However, unlike the classical adaptive control method, extremum seeking does not require a model. Instead, it uses the gradient of the defined cost function (e.g., SNR) to drive the set point of a dynamic system to its globally optimal location. Extremum seeking is desired when the set point of a system is unknown and/or varies with different conditions in a complex way that is known to have an extremum point, and the objective function of the system is to select the set point to keep the output at the extremum point.

Extremum seeking is particularly useful in applications where there are no reliable models such as in the area of fluid flow, combustion, and biomedical systems.

Back in the 1950s and 1960s, a significant effort was invested into the research on extremum seeking controllers. However, the resulting controllers turned out to be very complex and expensive to implement at that time. Also, it was not possible to guarantee the stability of the system although the extremum seeking controllers performed quite well when put into practice. As a result, research into extremum seeking died down and it only regained its popularity in the 21st century after Krstic published articles on the stability criterion for an extremum seeking system [4]. Since then, extremum seeking controllers have been used in applications such as compressor instabilities in jet engines, combustion instabilities, thermoacoustic coolers, beam matching in particle accelerators, and many more [5].

2. Extremum Seeking – How Does it Work?

Figure 1 shows the standard extremum seeking control architecture. A sinusoidal perturbation signal ($\alpha \sin(\omega t)$) is injected into the plant to get an estimate of the gradient information of the cost function. The output of the plant is given in the form:

$$J(\theta) = J^* + \frac{J''}{2}(\theta - \theta^*)^2 \quad (2.1)$$

The objective of the algorithm is to make the estimation error $\tilde{\theta} = \theta^* - \hat{\theta}$ as small as possible so that the output is driven to its minimum J^* . The output signals $J(\theta)$ are applied to a high-pass filter which removes the constant offset, demodulated by multiplication with $\sin(\omega t)$, and passed through an integrator which takes out the high frequency signal terms. The final output is a gradient estimate of the plant of the form:

$$\dot{\tilde{\theta}} \approx -\frac{k\alpha f''}{2}\tilde{\theta} \quad (2.2)$$

When the gradient $\dot{\tilde{\theta}}$ goes to zero, the estimation error $\tilde{\theta}$ goes to zero and the plant output is driven to its minimum J^* . The formal discussion on extremum seeking controllers, which includes stability proofs, can be found in [4].

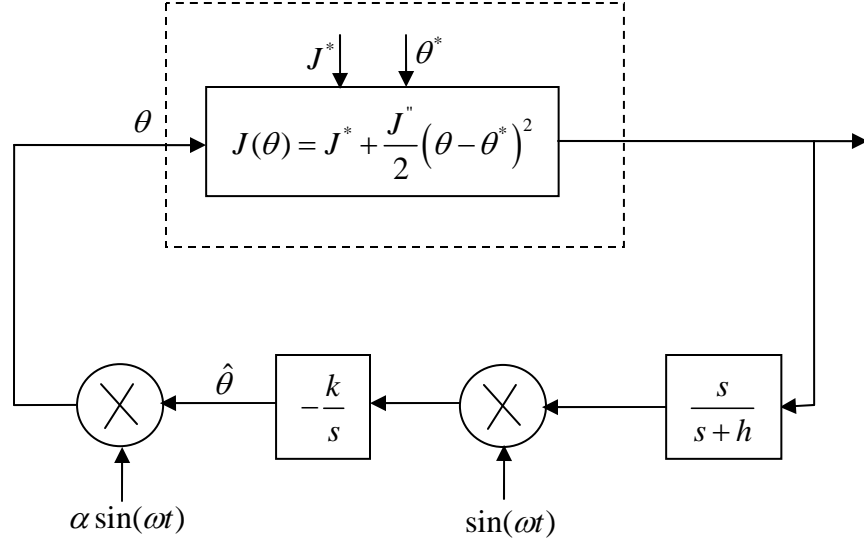


Figure 1. Perturbation-based Extremum Seeking Architecture [From Ref. [5]].

B. AUTONOMOUS VEHICLE COMMUNICATIONS NETWORKS

Electromagnetic wave propagation over a wireless communication network is random, unreliable, and attenuated by many loss mechanisms. The transmission path can vary from a simple LOS path to one that is highly attenuated by the ever-changing environment such as mountains and foliage. It is difficult to predict or accurately model the path loss, received signal power, and SNR at the receiver, especially if the receiver is moving.

If the receiver signal power is lower than the receiver's sensitivity, the receiver might not be able to detect and demodulate the messages, resulting in link breakage. The link margin measures the difference (in dB) between the received power and the receiver's sensitivity. The receiver's sensitivity is a characteristic of the system and is provided by the system's manufacturer.

$$\text{LinkMargin} = P_r - R_{\text{sens}} \quad (2.3)$$

A high link margin is preferred as this means that the received power is higher than the receiver's sensitivity and the receiver should be able to detect the messages.

In most communication network systems, it is desirable to maximize the received signal power. The link quality of the communication network is not dependent on the received signal power alone. It is also dependent on the noise level of the system. There are various sources of noise in the communication system which can come from the environment and system devices. If the noise power is near or higher than the received signal power, it is difficult for the receiver to detect the signal among the noise-contaminated received signal. Hence, besides having a large signal power, it is desirable to have a low noise power.

Signal-to-noise ratio (SNR) is a measure of the ratio between the received power and the noise power. The higher the SNR, the larger the signal level as compared to the noise level, resulting in a lower bit error rate in signal reception and better link quality.

$$SNR = \frac{ReceivedSignalPower}{NoisePower} \quad (2.4)$$

The SNR is related to channel capacity by the Shannon-Hartley theorem [6]. The theorem states that the theoretical maximum channel capacity (C , in bits per second) is proportional to the SNR and the bandwidth (W , Hz) of the channel as shown in Equation 2.5.

$$C = W \log_2(1 + SNR) \quad (2.5)$$

Assuming that the capacity of the channel is fully utilized (i.e., capacity equals to the throughput), an increase in SNR will lead to an increase in the throughput of the channel.

1. Propagation Mechanisms

The mechanisms behind electromagnetic wave propagation are diverse, but can generally be attributed to direct line-of-sight (LOS) path, reflection, deflection, and scattering [7]. The losses associated with these mechanisms are briefly discussed in this section and the propagation models, which describe these mechanisms, are discussed in the next sections.

a. Friis Free Space Equation

The free space power received by the receiver antenna can be described by the Friis free space equation.

$$P_r = \frac{P_t G_t G_r \lambda^2}{(4\pi)^2 d^2 L} \quad (2.6)$$

where P_t is the transmitted power, G_t is the transmitter gain, G_r is the receiver gain, λ is the wavelength in meters, d is the transmitter-receiver separation distance in meters, and L is the system loss factor not related to propagation. L is assumed to be 1 for a lossless system.

Equation (2.6) is used to compute the free space path loss when the transmitter and receiver have a clear, unobstructed line of sight path between them. The equation shows that the received power is inversely proportional to the square of the separation distance.

The free space path loss, which represents signal attenuation as a positive value measured in dB, is defined as the difference (in dB) between the transmitted power and the received power given by equation (2.7). The antenna gains are assumed to have unity gains in the path loss equation.

$$L_p \text{ [dB]} = P_r - P_t \text{ [dB]} = 32.4 + 20 \log(f) \text{ [MHz]} + 20 \log(d) \text{ [km]} \quad (2.7)$$

The free space path loss is generally the most important loss parameter affecting wave propagation in the radio channel.

The Friis free space equation can be written by combining equations (2.6) and (2.7) as follows

$$P_r \text{ [dB]} = P_t + G_t + G_r - L_p \quad (2.8)$$

b. Antenna Gain Patterns

Generally, the antenna gains are not constant around the azimuth and elevation of an antenna. Figure 2 shows the antenna gain patterns of a vertically polarized

sector antenna from Laird Technologies (SA24-120-9). In the elevation direction, the 3 dB beam width is ± 15 degrees and the gain drops off sharply after ± 15 degrees, reaching -22 dB at a 30 degree angle. The received power will be significantly lower if the LOS path is outside the beam width of the antenna, which indicates a loss of coverage from the antenna. The attenuation can easily be computed by doing a ray-tracing of the wave propagation path between the transmitter and the receiver to determine the angle of the departure/arrival of the ray-path.

The antenna gain pattern loss (LAP) can be accounted for in the Friis free space equation by adding a term LAP to equation 2.8 as follows,

$$P_r[dB] = P_t + G_t + G_r - L_p - L_{AP} \quad (2.9)$$

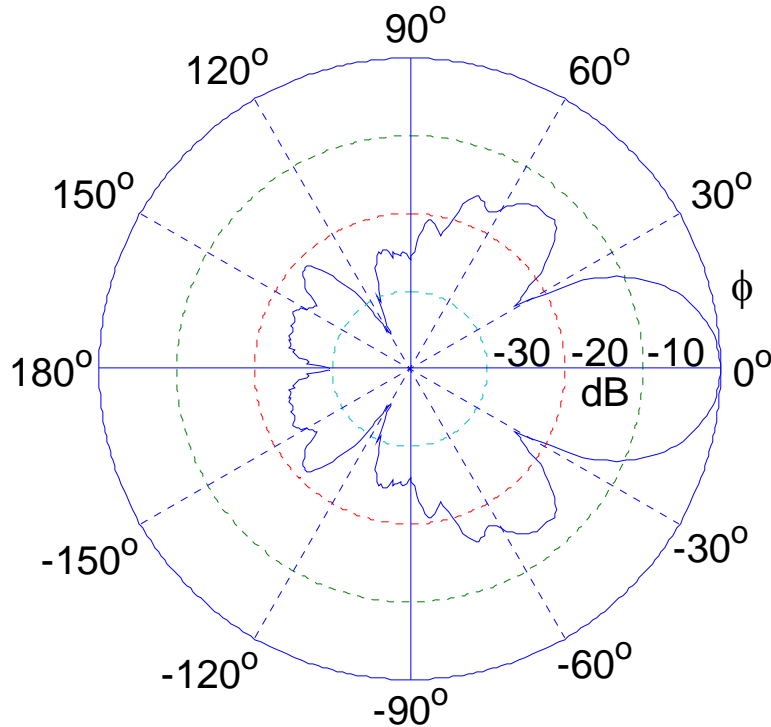


Figure 2. Antenna Pattern for Vertical Polarized Sector Antennas from Laird Technologies (Model SA24-120-9).

c. Reflection

Reflection occurs when a propagating electromagnetic (EM) wave hits an object that has very large dimensions when compared with the wavelength of the propagating EM wave. Reflection usually occurs off the earth's surface, mountains, and buildings.

When the propagating EM waves hit the reflective surface, part of the energy is transmitted into the second medium, part of the energy is reflected back to the air, and a small part of the energy is loss in absorption. The reflection follows the Snell's law of reflection. The amplitude and phase of the reflected wave depend on a number of variables, including dielectric constant of the surface, frequency, polarization, and angle of incidence [7].

d. Diffraction

Diffraction occurs when the propagating EM wave hits a surface that has sharp irregularities (edges). Secondary waves will originate from the sharp irregularities and propagate throughout the free space and behind the obstacle, bending waves around the obstacle (Huygen's Principle). Diffraction allows the receiver to receive signals outside the LOS path with the transmitter.

Generally, it is difficult to model diffraction losses accurately as it requires a detailed knowledge of the terrain profile and the computation is difficult from a mathematical perspective. Expressions for diffraction losses for many simple cases are available and they are usually theoretical approximations modified by empirical corrections. Ref. [7] contains a description of some simple models developed to estimate diffraction losses.

e. Scattering

Scattering occurs when the propagating EM wave hits particles with dimensions that are small compared to the wavelength, and where the number of particles per unit volume is large. Example of such particles would be snow, fog, and rain.

Scattering losses become a significant source of losses (where attenuation is more than 1 dB) above 10 GHz and is not significant at 2.4 GHz. Scattering losses from fog and snow become noticeable above 30 GHz and for rain attenuation at around 10 GHz [7].

2. Propagation Models

Propagation models are primarily used to predict the path loss, received signal strengths, and from there the SNR of the communication system. There are many propagation models available such as the Two-Ray Model, Log-distance Path Loss Model, Longley-Rice Model, and the Hata Model [7]. These models vary widely in their approach, application, complexity, and accuracy. Generally, these models can either be categorized into analytical or empirical models, or a combination of both.

The empirical model is based on curve fitting or an analytical expression that recreates a set of measured data. While the empirical model has the advantage of taking into account all propagation factors through actual field measurements, the validity of the model in environments other than those used to derive the model is always an issue. The model is considered only useful in the new environment if measurements are taken and the model is validated in the new environment.

The analytical model uses the ray-tracing technique and terrain geometry (from aerial photographs, Geographical Information System (GIS) databases, or other similar databases) to deterministically compute the path loss of the propagation channel. Using the ray-tracing technique, it is possible to determine all ray-paths of the EM waves and their field properties (amplitude, phase, and time of arrival) between the transmitter and receiver. The received signal intensity is the summation of the signal intensity for each ray-path. The accuracy of the analytical model depends on the resolution of the terrain database.

C. PROPOSED THEORETICAL PROPAGATION MODEL

Electromagnetic wave propagation over a wireless communication network is extremely random and is driven by the many loss parameters described above as well as the terrain profile. For a start, it is difficult to account for and model all the loss

parameters and the terrain accurately. In this project, the author is going to develop a SNR model that is suitable for application at hand. The model will focus on two dominant loss parameters, namely the LOS path loss and the antenna gain pattern loss. In addition, the author is going to model the effect of the UAV orientation on the SNR. The ray-tracing technique will be used to compute the LOS path between the transmitter and receiver. The terrain is assumed to be flat with no features.

THIS PAGE INTENTIONALLY LEFT BLANK

III. FLIGHT CONTROL SYSTEMS

A. SIG RASCAL 110 AIRPLANE

The Rascal 110 airplane (shown in Figure 2) is a hobby-class prefabricated airframe with ample room for additional avionics in the cabin. This highly configurable system allows the installation of additional avionics to support testing of new hardware, algorithms, and technical solutions [8].



Figure 3. Rascal Unmanned Aerial Vehicle (UAV)

The Rascal airframe was converted at NPS into a fully autonomous UAV equipped with the following:

- Cloud Cap Technology Piccolo+ autopilot avionics
- PC-104 onboard computers (x2)
- 900 MHz radio modems for ground control station (GCS) link
- 2.4 GHz Wave Relay wireless networking card
- Single-axis high resolution camera
- GPS and pilot-static probe
- Pelco network digital video server

B. WAVE RELAY WIRELESS MESH NETWORK

In addition to the 900 MHz wireless link dedicated to the safe operation of multiple UAVs from one ground control station, a second wireless link, namely the Wave Relay wireless networking system operating in a 2.4 GHz 802.11 mesh network, was added to the Rascal UAV in FY08. The second wireless link expands the capability of the UAV and allows for the development and execution of various non-critical and/or real-time applications on the UAV.

On the Rascal UAV, this wireless link is facilitated by a Wave Relay radio mounted on a single board computer card. The radio is connected to a 3 dB omnidirectional antenna mounted on the belly of the UAV for transmitting and receiving messages. On the GCS, the wireless link is facilitated by a Wave Relay radio router as shown in Figure 2. The Wave Relay router on the GCS is paired with three 9 dB sector antennas to provide 360 degrees of azimuth coverage.

The specification on the Wave Relay radio as provided by the manufacturer states that the transmit power of the Wave Relay radio is around 28 dB and the receiver sensitivity is around -74 dBm. In a normal environment, a noise floor of around -95 dBm is assumed, but it can be worse than that depending on the operating environment.

The datasheets for the antenna used in this project are attached as Appendix A.



Figure 4. Wave Relay QAUD Radio Router [From [9]].

IV. MODELLING

A. SNR MODEL (MULTI-NODES)

The SNR model shown in Figure 5 was developed using MATLAB Simulink 6.3. The inputs to the model are the UAV flight trajectory and the location of the ground nodes. The model outputs are the received power, SNR, and link margin at the receiver. The model computes the LOS path between the UAV and the ground node, and from there the model computes the free-space LOS path loss, antenna pattern loss, and the effect of the UAV bank angle on the SNR. The terrain is assumed to be flat with no features.

The current model accepts up to two ground nodes and one UAV. However, the model can be easily modified to accept more ground nodes and UAVs. The measurement units used in the model are System Internationale (SI) units.

The SNR model consists of the following four sub-models:

- UAV Dynamic Model
- LOS Path Loss Model
- Antenna Pattern Loss Model
- Link Budget Model

The function of each sub-model will be briefly described below.

1. UAV Dynamic Model

The UAV dynamic model (Figure 6) models the flight trajectory of the UAV. The inputs are speed and heading rate and the outputs are position, velocity, heading, and bank angle of the UAV in flight.

The position and velocity are defined in the east-north-up (x-y-z) local tangent plan coordinate system. The heading is defined with 0 degrees east and rotates anti-clockwise. The positive bank angle corresponds to the left wing (seen from front) being raised above the horizon plane.

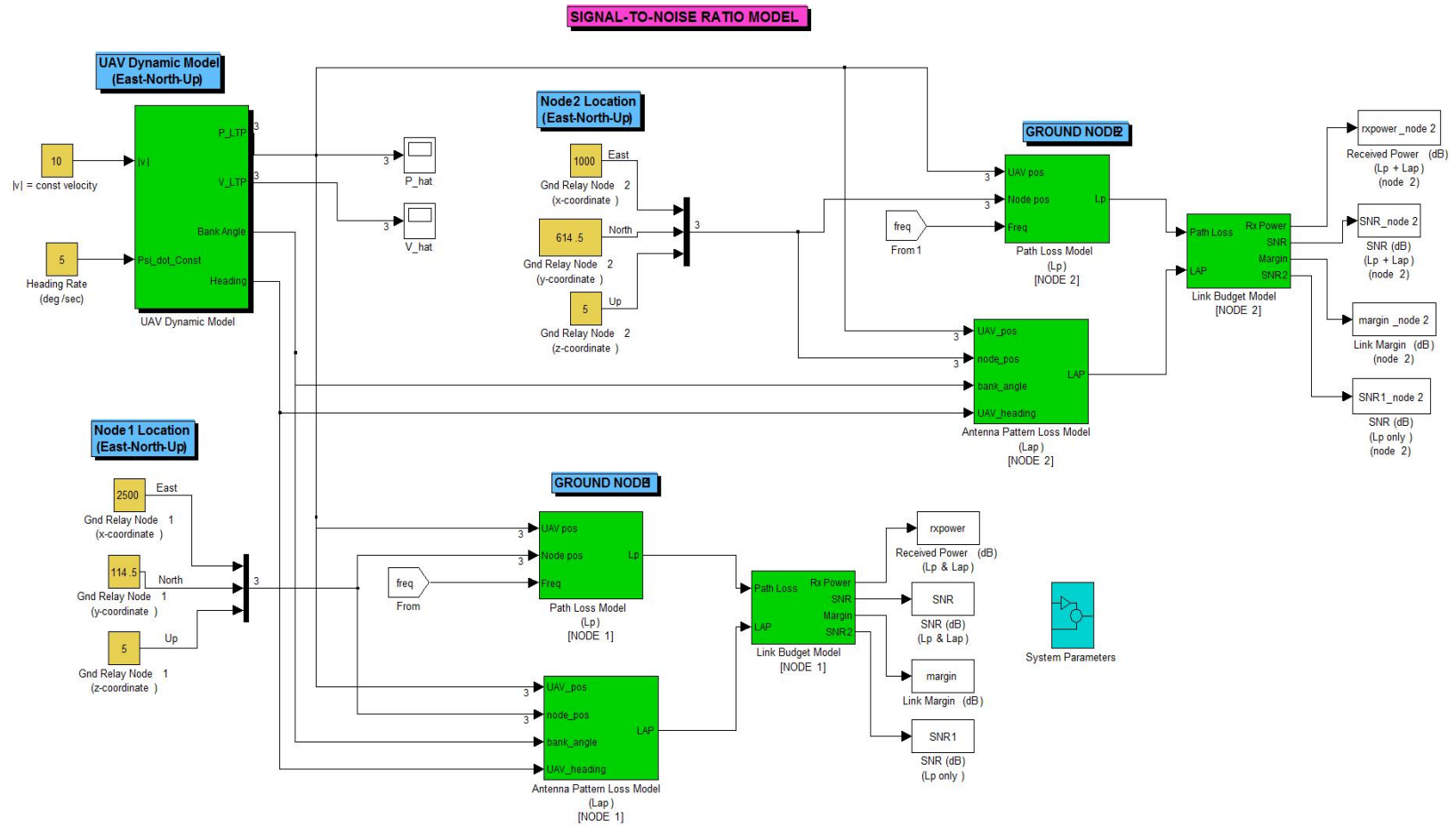


Figure 5. SNR (Multi-Nodes) Model.

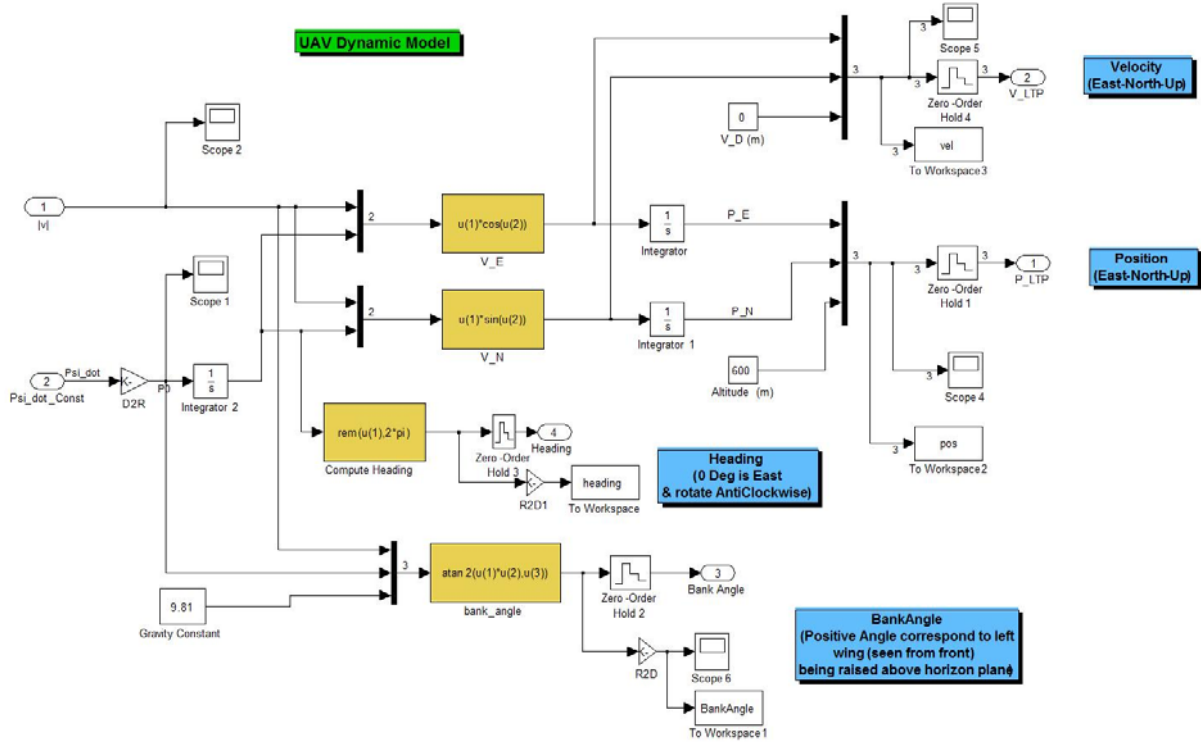


Figure 6. UAV Dynamic Model.

2. LOS Path Loss Model

The LOS path loss model shown in Figure 7 computes the difference between the transmitted power and received power (excluding the effect of antenna gain) of the LOS path. The path loss is computed using the Friis free space equation as shown below.

$$PathLoss = L_p = 32.4 + 20 \log(f)[MHz] + 20 \log(d)[km] \quad (4.1)$$

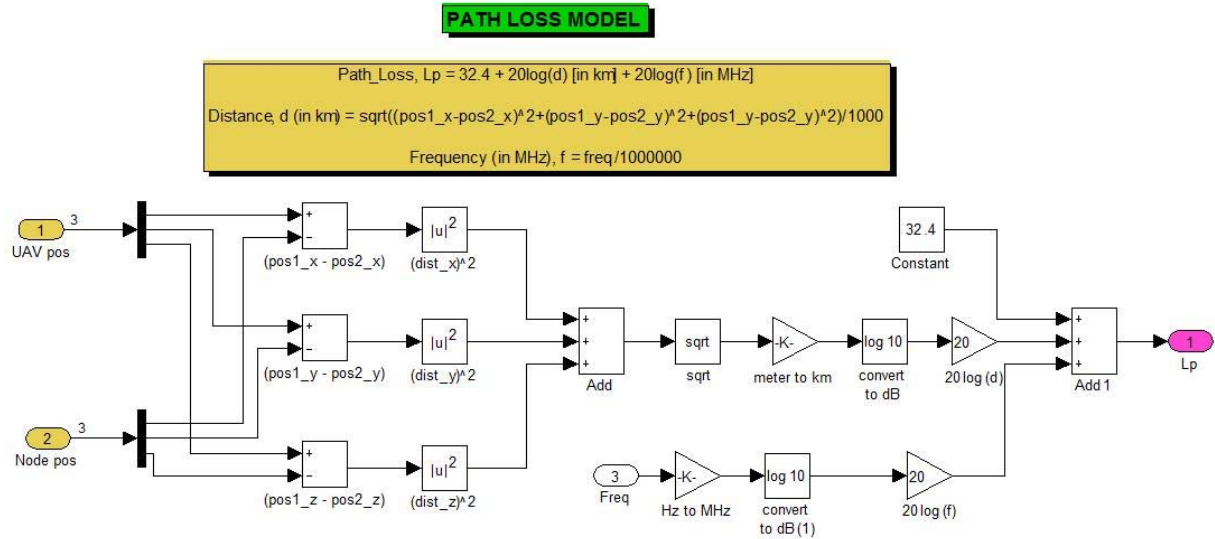


Figure 7. Path Loss Model.

3. Antenna Pattern Loss Model

The antenna pattern loss model (Figure 8) computes the departure and arrival angles of the LOS path and then determines the antenna pattern losses using a look-up table.

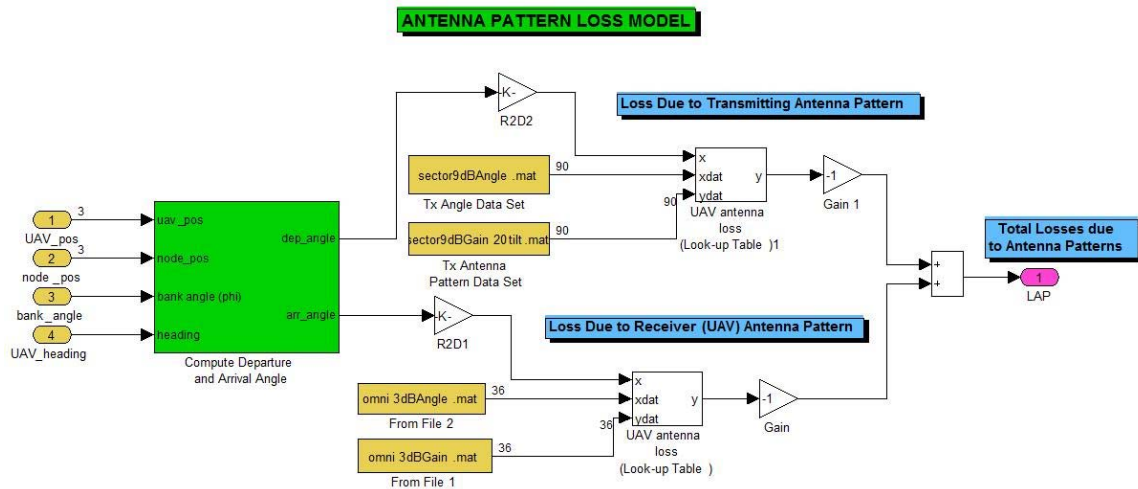


Figure 8. Antenna Pattern Loss Model.

The arrival angle is affected by the bank angle of the UAV. As shown in Figure 9, the bank angle has the effect of moving the incident ray path along either side of the

plane and increases or decreases the angle of arrival. The bank angle effect is “greatest” when the UAV is perpendicular to the ground node and has no effect when the UAV is in head-on or tail-chase scenarios.

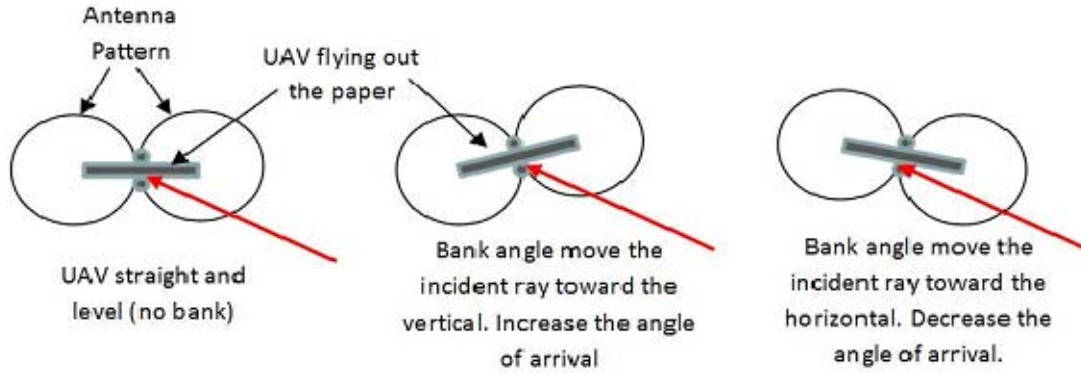


Figure 9. UAV Bank Angle Effect on the Arrival Angle.

The effect of the bank angle on the arrival angle is accounted in the model by a “sin” term as shown below:

$$BankAngleEffect = \phi * Sin(\varphi - \lambda) \tag{4.2}$$

where ϕ = UAV’s bank angle

φ = bearing, angle between positive x-axis and the ground projection of the LOS ray path.

λ = UAV’s heading

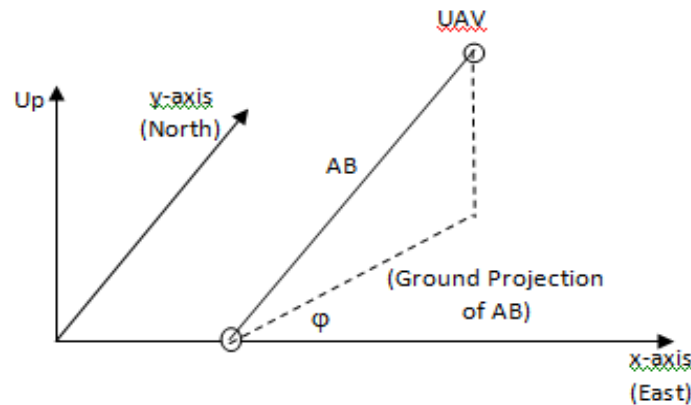


Figure 10. Geometry Showing the Definition of Bearing, φ

The antenna pattern is usually obtained through field measurements of the antenna. In this project, the author stored the antenna gain (obtained from the manufacturer’s datasheet) in a look-up table, and the gain at particular departure and arrival angles are obtained from the look-up table using linear interpolation. It is also possible to do curve-fitting to obtain an analytic expression for the antenna pattern. The author tried this method and compared the results with the look-up table. It was found that the error between the two methods is not significant.

4. Link Budget Model

The link budget model seen in Figure 10 computes the received power (P_r), signal-to-noise ratio (SNR), and link margin at the receiver. In addition, the SNR excluding the antenna pattern loss is also computed.

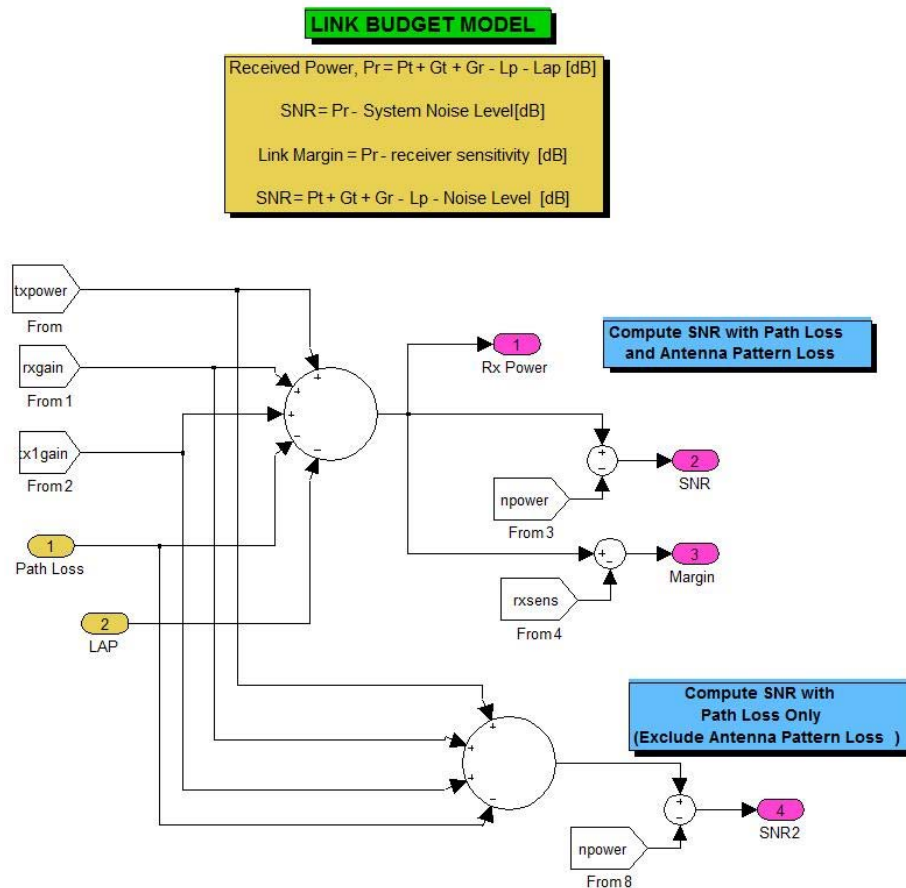


Figure 11. Link Budget Model.

The equations used in the model are as follows:

From equation 2.9,

$$P_r[dB] = P_t + G_t + G_r - L_p - L_{AP} \quad (4.3)$$

From equation 2.4,

$$SNR[dB] = P_r - NL \quad (4.4)$$

From equation 2.3,

$$LinkM \text{ arg in}[dB] = P_r - R_{sens} \quad (4.5)$$

The SNR_{PL} excludes losses due to antenna pattern effect and only account for the LOS path loss

$$SNR_{PL}[dB] = P_t + G_t + G_r - L_p - NL \quad (4.6)$$

where P_t = transmit power (28 dBm)

G_t = transmitter antenna gain (9 dB)

G_r = receiver antenna gain (3 dB)

L_p = LOS path loss (dB)

L_{AP} = antenna pattern loss (dB)

NL = system noise level (-95 dBm)

R_{sens} = receiver sensitivity (-74 dBm)

The transmit power, antenna gains, noise level, and receiver sensitivity are characteristic of the radio and antenna systems and are obtained from the system's datasheet.

B. RASCAL SNR MODEL

The Rascal SNR model (Figure 11) is similar to the above SNR model except that the inputs are modified to accept actual flight test data from the Rascal's telemetry.

A first-order filter is implemented to filter off the high frequency variations in the SNR readings. The filtered SNR data is used as input to the extremum seeking algorithm. The author tried using second-order filters and a weighted moving average (20 points) to filter off the high frequency variation, but it was found that the first-order filter performs better and is more suitable for the author's application.

C. SNR MAP

The SNRmap.m is a script file written in MATLAB. The SNR map shows the variations of SNR in X-Y coordinates for a stationary (non-dynamic) UAV. The altitude, heading, and bank angle of the UAV are fixed before the run and can not be changed during the run. Figure 12 (X-Y Plane) and Figure 13 (X-Z Plane) show the SNR map for a typical run. The SNR map is very useful for plotting contour maps.

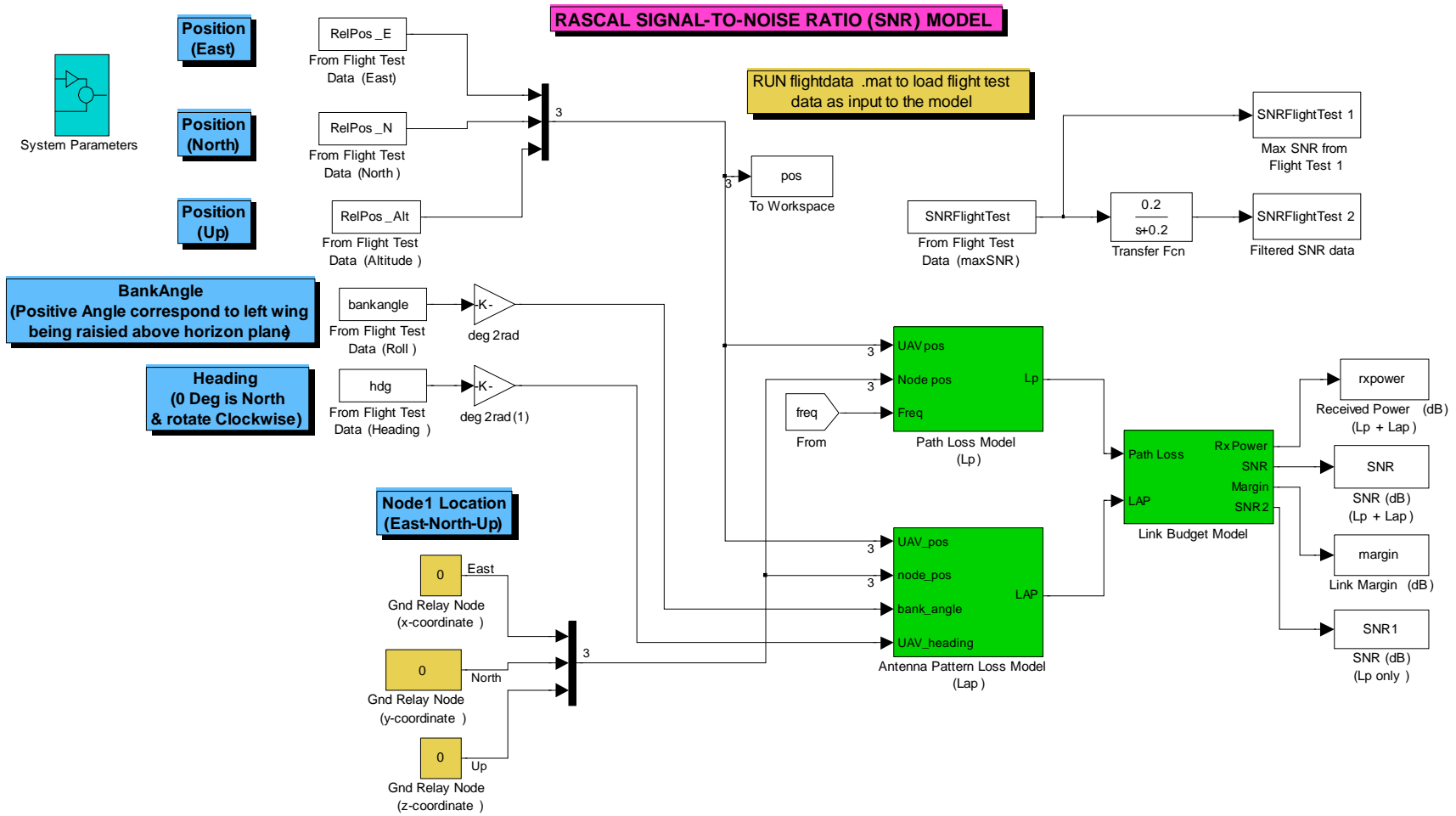


Figure 12. RASCAL SNR Model.

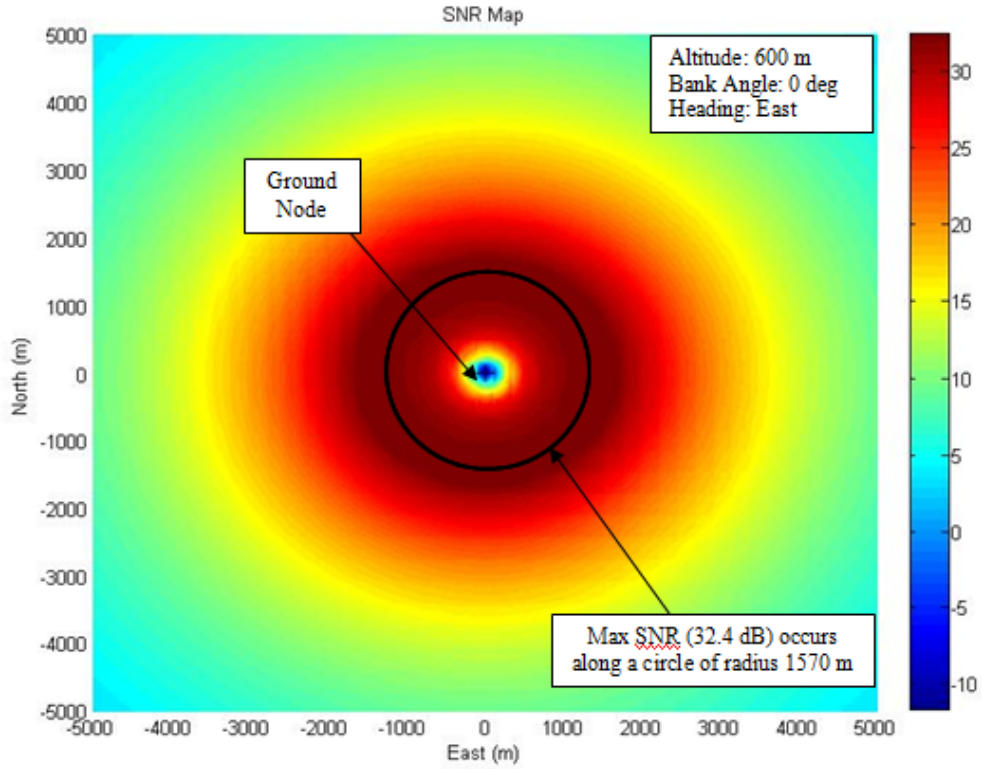


Figure 13. SNR Map (X-Y View).

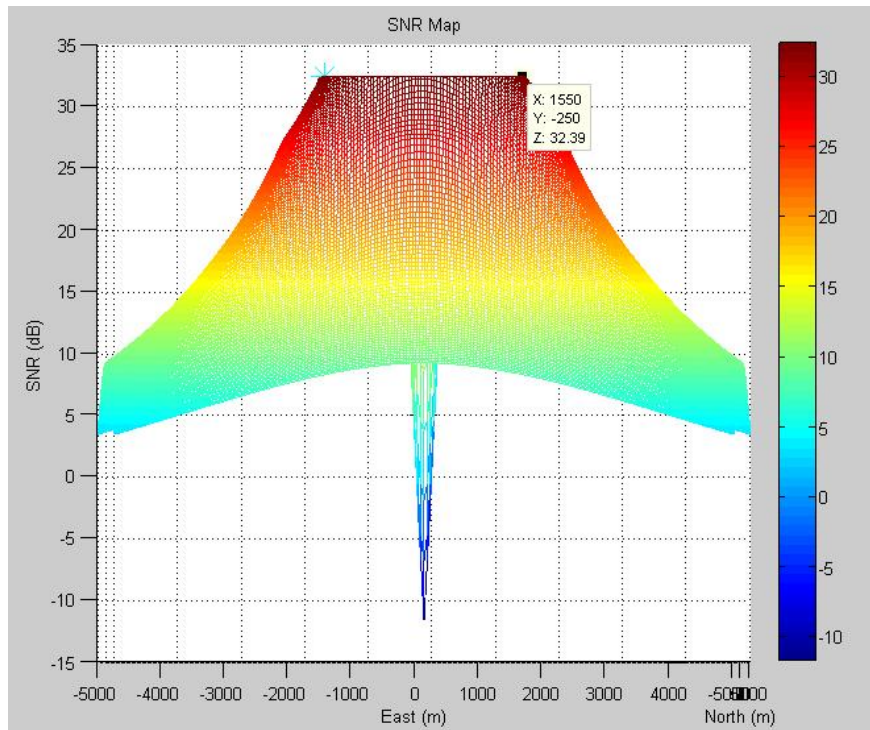


Figure 14. SNR Map (X-Z View).

V. SNR MODEL VERIFICATION FLIGHT TEST

A. BACKGROUND

The SNR model verification flight test with the Rascal UAV was conducted at McMillan Air Field in Camp Roberts, California on August 1, 2008. The primary objective was to collect SNR measurements between the Rascal UAV and a ground control station (GCS) node at different locations and altitudes. The SNR measurements obtained from the flight test will be used to validate the mathematical SNR model.

The flight test data were obtained from two separate sources. The SNR data was obtained by the SNR logger from the Wave Relay network while the UAV flight parameters (such as latitude/longitude, altitude, roll, yaw and pitch) were obtained from the Piccolo onboard the Rascal UAV. These two sources of data were synchronized using the time stamp found on both data sets. For plotting purposes, the position of the GCS node is fixed as the origin of the local tangent plane (east-north-up) coordinate system.

B. SET-UP

The set-up for the flight test was as follows:

Ground Control Station Node

Antenna: 3 x 9 dB vertically polarized sector antenna (SA24-120-9)

Position¹: 35.7167 (lat) / -120.7648 (lon) (refer to Figure 12)

Altitude¹: 272m (above mean sea level)

Rascal UAV

Antenna: 2.2 dB omni-directional antenna (HG2402RD-RSF)

Flight Paths: As shown in Table 1 and Figure 12

¹ Extracted from Google Earth.

Path	Description	Duration (sec)
A	2 x anti-clockwise circular orbit at altitude 560m	145
B	2 x anti-clockwise circular orbit at altitude 560m	150
C	1.5 x anti-clockwise circular orbit at altitude 650m	130
D	1.5 x anti-clockwise circular orbit at altitude 650m	100
E	1 x anti-clockwise circular orbit at altitude 650m	100
F	1.5 x anti-circular orbit at altitude 500m	140
F	2 x anti-circular orbit at increasing altitude from 500m to 700m	150

Table 1. Flight Paths of Rascal UAV during Flight Test.

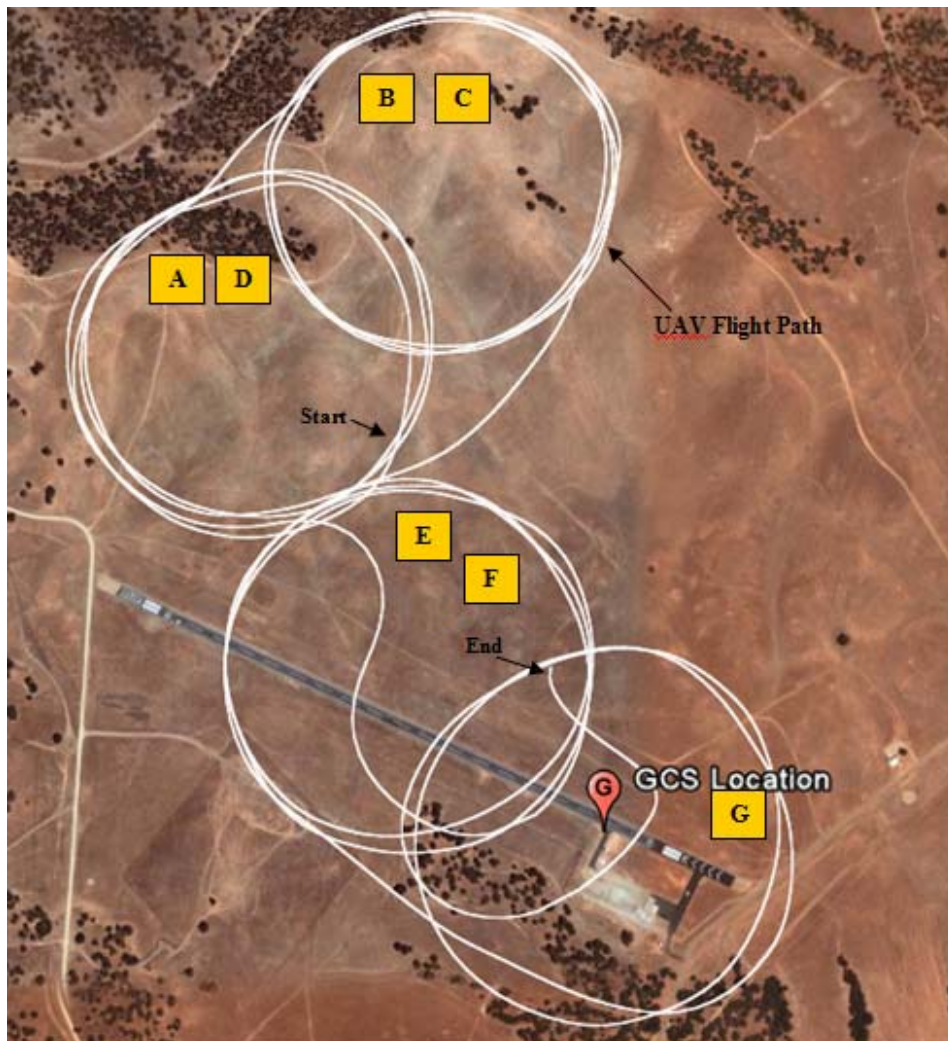


Figure 15. Location of GCS and Rascal Flight Paths during Flight Test [From Google Earth].

C. FLIGHT TEST RESULTS AND ANALYSIS

1. SNR Variation with Distance

Figure 15 (3D) and Figure 16 (2D) show the SNR measurements recorded on the GCS node. From these figures, it is observed that the SNR generally decreases with the radial distance between the UAV and GCS in paths A, B, C and D of the flight trajectory. However, at paths E, F & G nearer to the GCS (radial distance < 350 m), there are some “unusual” fluctuations in the SNR reading. These fluctuations may be due to the multipath effect of the environment and/or the UAV flying outside the main beam width of the GCS antenna which affects the received power.

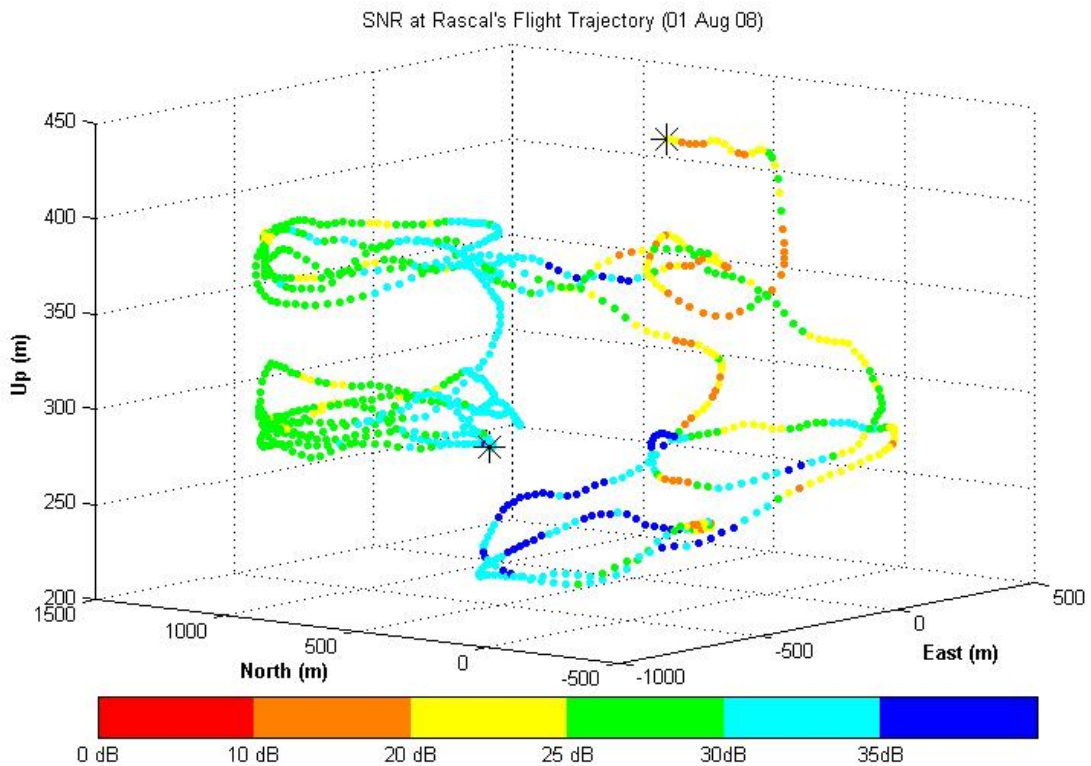


Figure 16. Actual SNR Readings along the Rascal Flight Trajectory (3D map) Obtained during Flight Test.

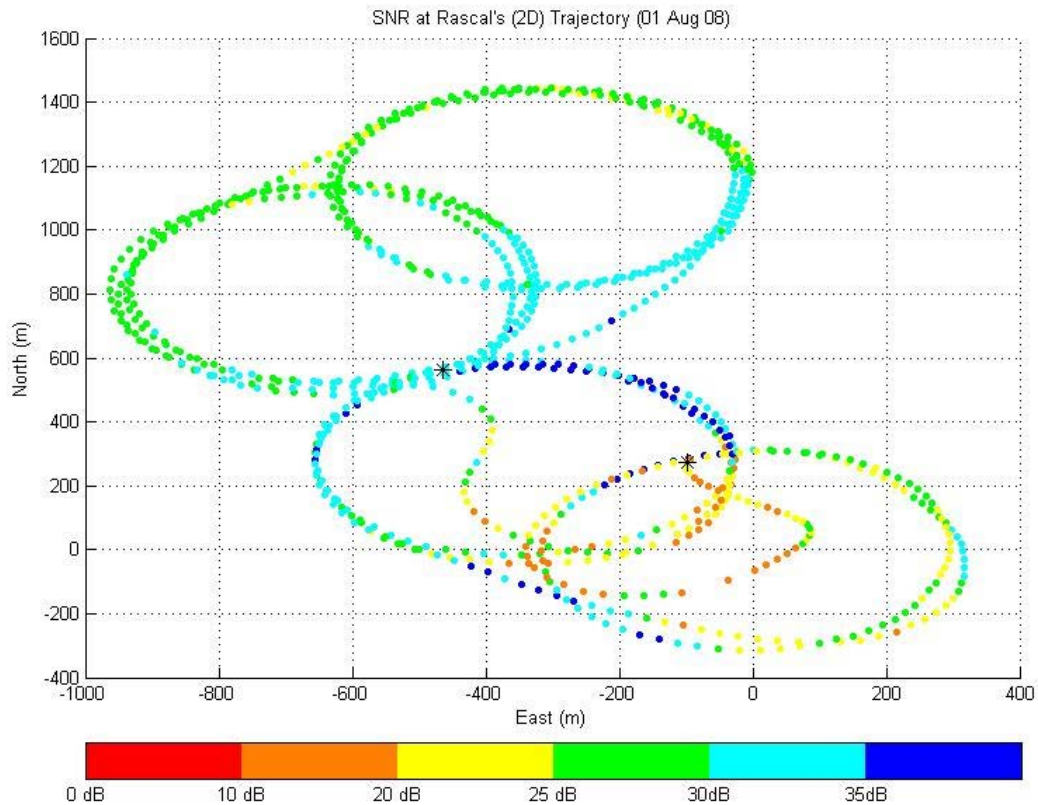


Figure 17. Actual SNR Readings along the Rascal Flight Trajectory (2D map in east-north) Obtained during Flight Test.

2. SNR Variation with Altitude

Figure 17 shows the SNR variation with altitude for paths B and C. In paths B and C, the UAV flew the same circular path except for the difference in altitude of 100m. It is observed that the SNR does not vary significantly with a slight change in altitude when compared with radial distance. At a large radial distance, the range, arrival, and departure angles of the ray path do not change significantly with altitude and hence the losses and signal-to-noise ratios will be similar.

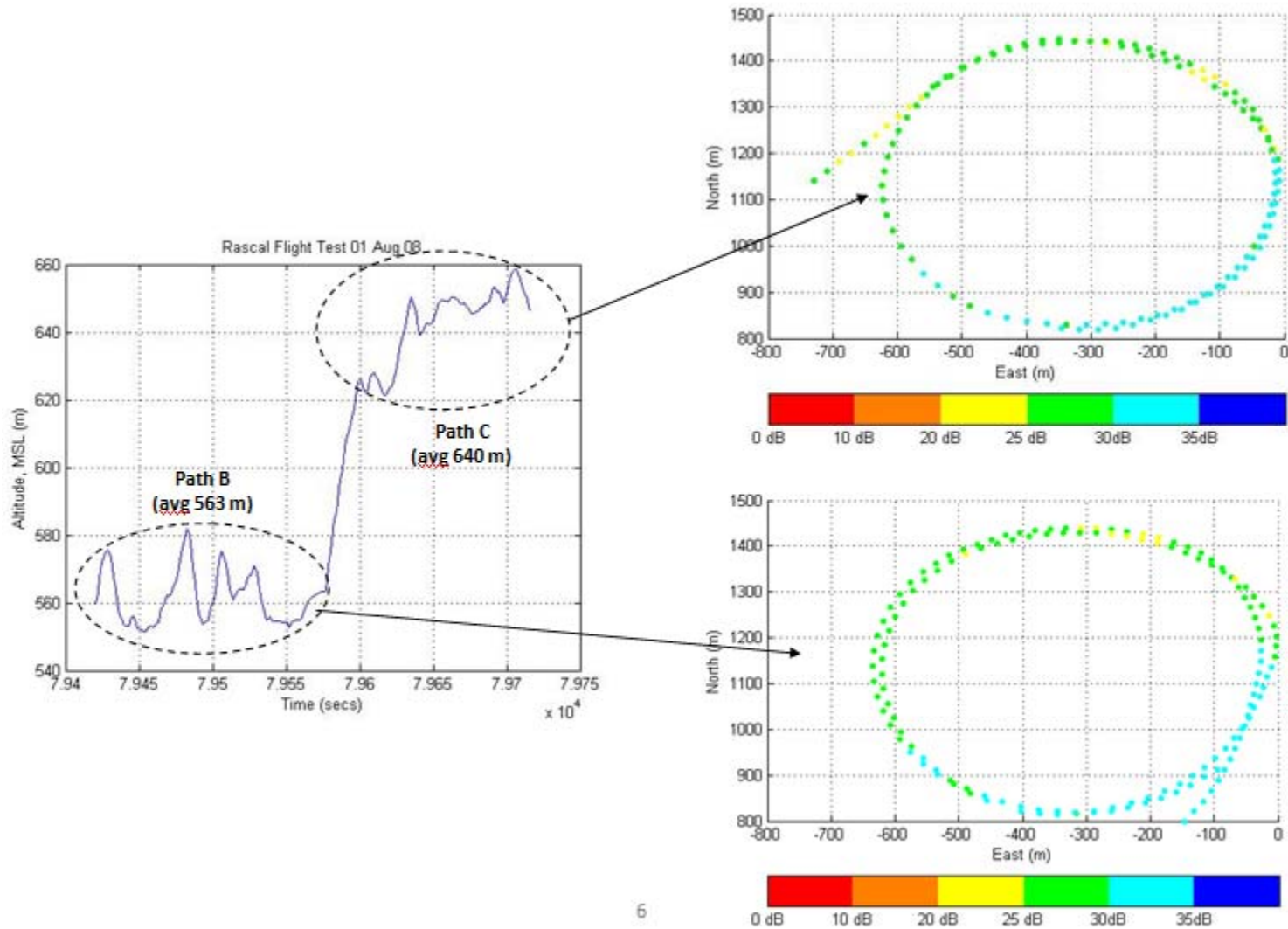


Figure 18. Variations of SNR Readings with Altitude at Paths B and C of the Flight Trajectory.

3. SNR Variation with GCS Antenna Pattern

Figure 18 illustrates the effect of the GCS antenna pattern on SNR readings on paths E and F of the flight trajectory. If the radial distance between the UAV and the GCS is short ($< 300\text{m}$ @ altitude $> 500\text{m}$), the UAV is likely to be flying outside the 15 deg main beam width of the GCS antenna. This effectively decreases the signal strength which leads to lower SNR values at the UAV.

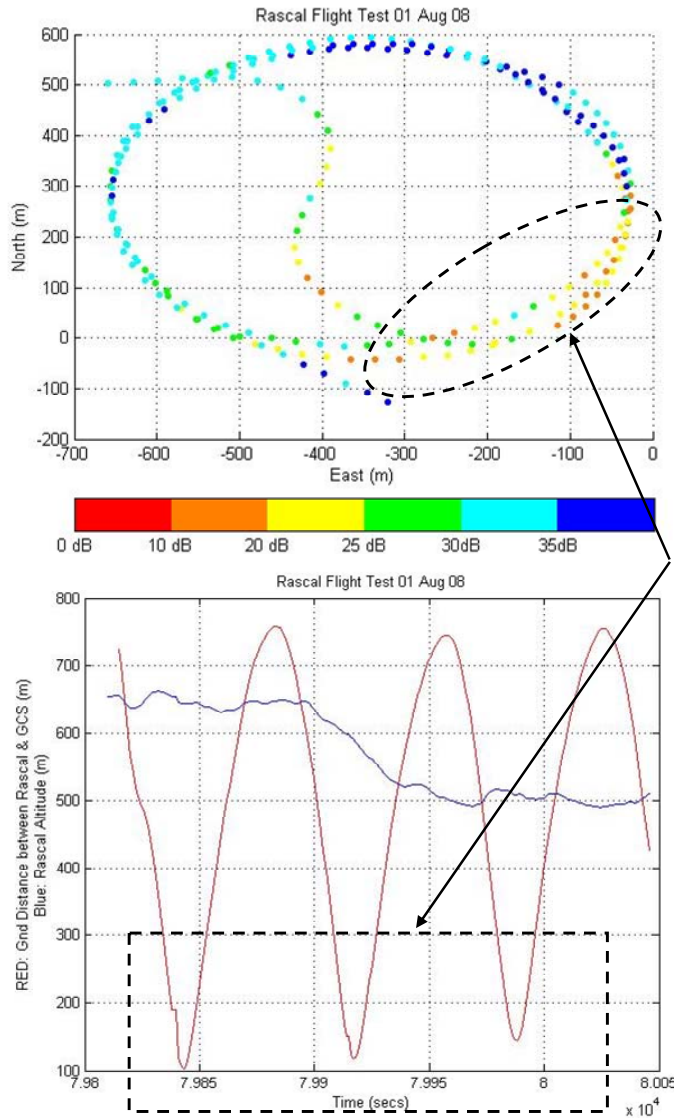


Figure 19. Variations of SNR Readings with the GCS Antenna Pattern of the Flight Trajectory.

4. Comparison of Actual Flight Test Data with Mathematical SNR Model

The position, heading, and bank angle information of the Rascal UAV were used to drive the mathematical Rascal SNR model. Figure 19 (3D) and Figure 20 (2D) show the SNR readings obtained from the mathematical SNR model. It is seen that at ranges far away from the GCS (paths A, B, C & D of the flight trajectory), the simulated SNR readings compared nicely with the actual SNR data from the flight test. The error of the simulated model with respect to the actual SNR test data in this region was within 15% (Figures 21 and 22). However, at ranges near the GCS (paths E, F & G of the flight trajectory) the error was more than 30%. The model predicted the UAV to be inside the GCS main beam width and hence should have had a reasonably high SNR in this region. However, the flight test reading showed otherwise. This inconsistency might be due to an inaccurate antenna pattern used in the model or because the signal attenuation at these regions is affected by multipath effect which was not accounted for in the model.

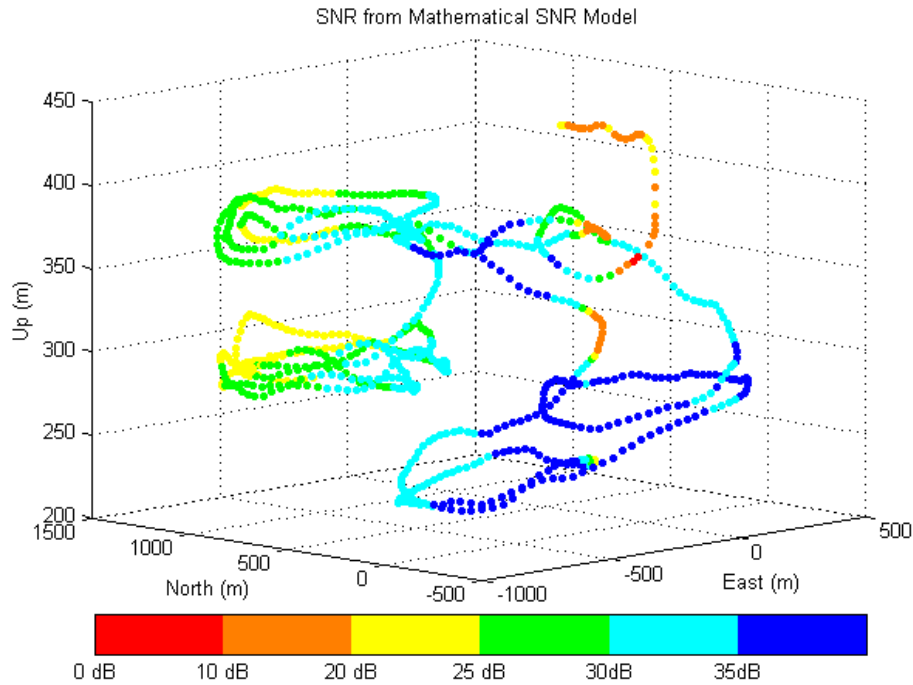


Figure 20. Simulated SNR Readings along the Rascal Flight Trajectory (3D map) obtained from Mathematical SNR Model.

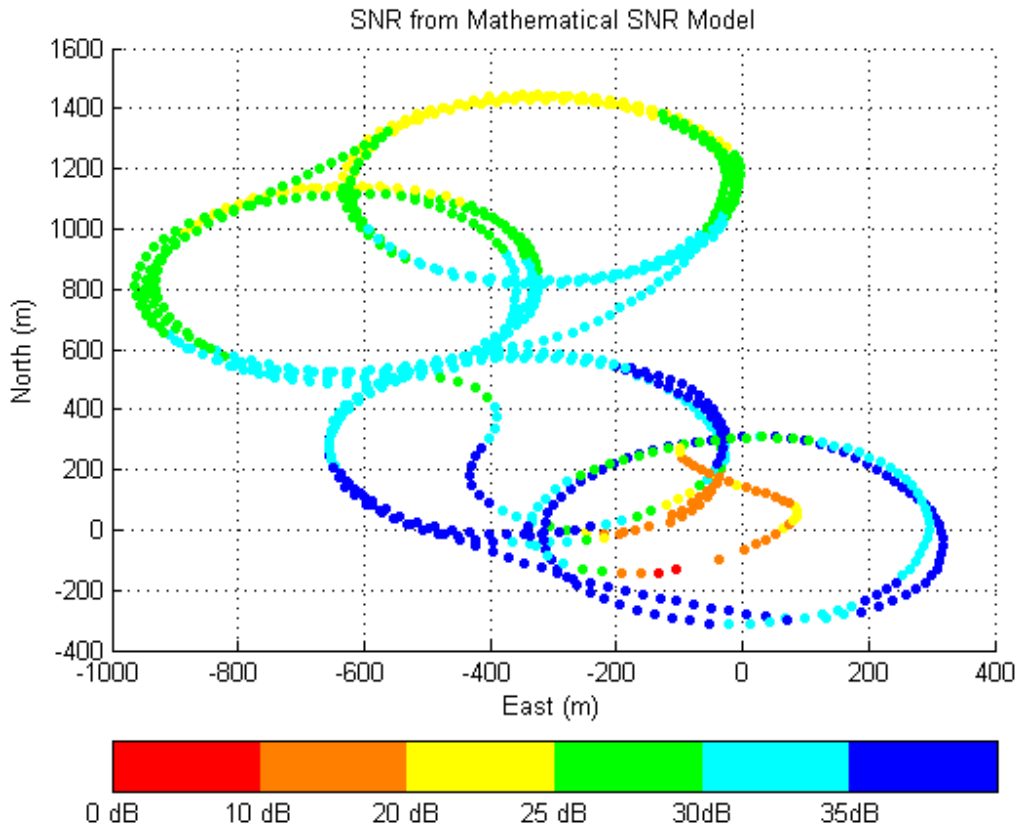


Figure 21. Simulated SNR Readings along the Rascal Flight Trajectory (2D map) obtained from Mathematical SNR Model.

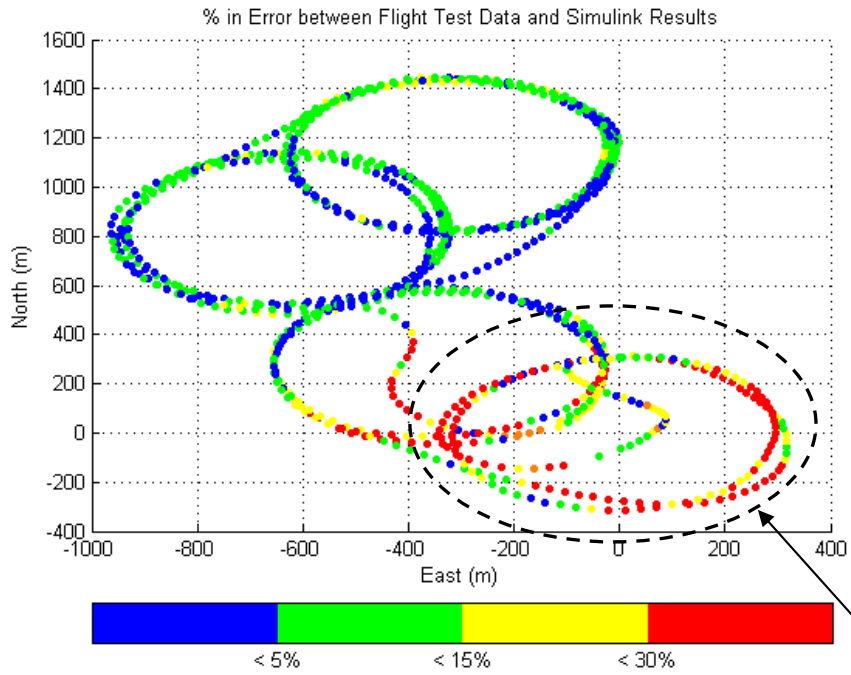


Figure 22. SNR Error (in %) between Simulated Reading and Actual Flight Data.

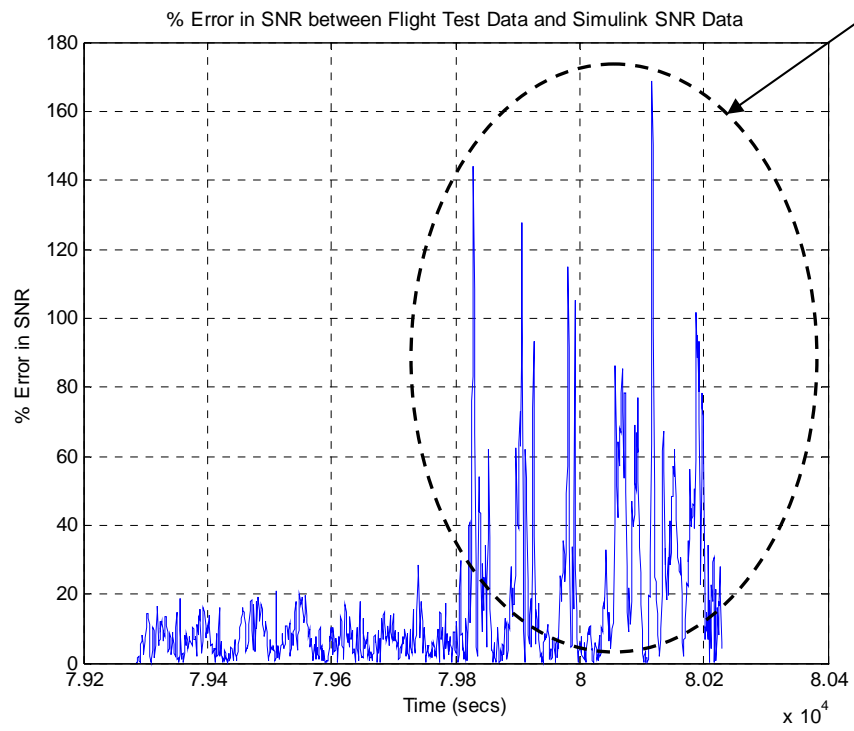


Figure 23. SNR Error (in %) Plotted Against Time.

5. Comparison of Actual Flight Test Data with SNR Map

The actual SNR data from the flight test were superimposed onto the SNR map as shown in Figures 23, 24, and 25. The SNR map was generated for the GCS node as the origin in east-north coordinates for a stationary UAV. The UAV altitude was set at 590m with zero bank angle and north heading.

It is clearly seen that the actual SNR data followed the general trends of the SNR map. The maximum SNR from the flight test occurred near the maximum SNR predicted by the model.

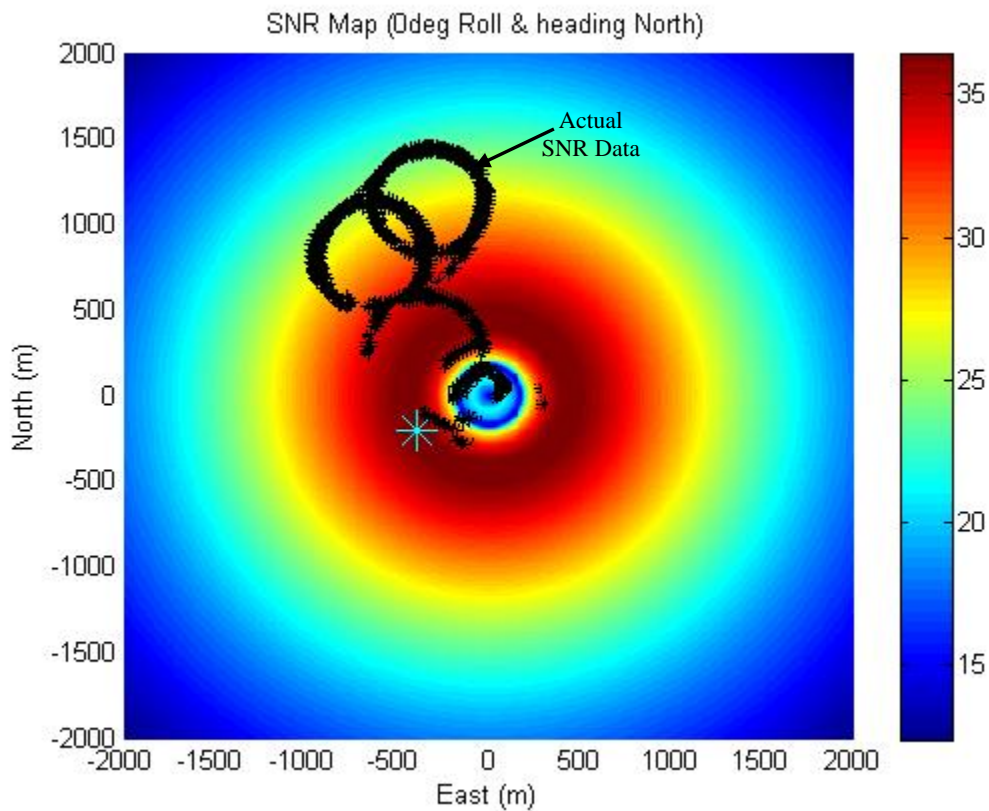


Figure 24. Actual SNR Data Superimposed onto the SNR Map (East-North View).

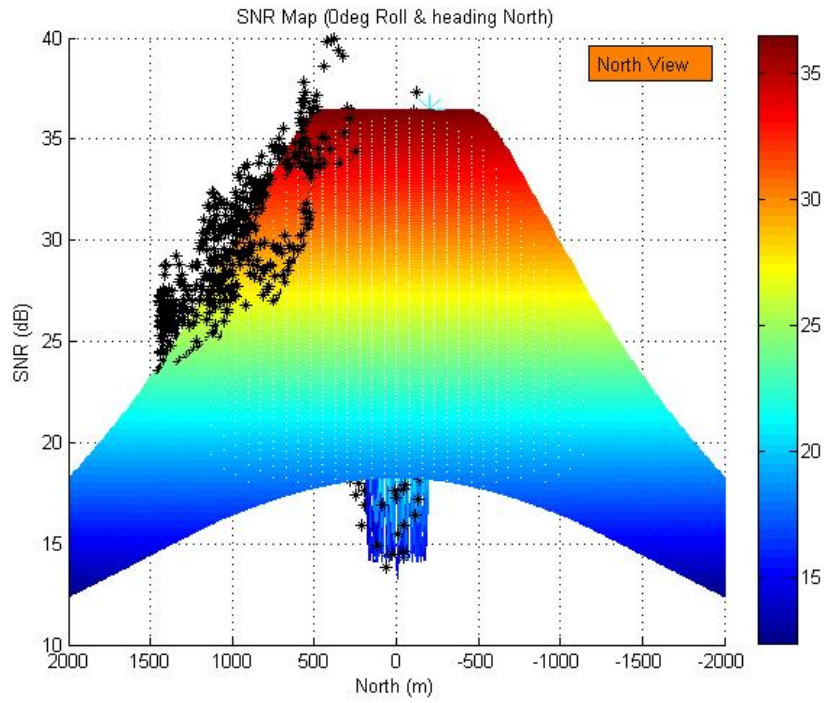


Figure 25. Actual SNR Data Superimposed onto the SNR Map (North View).

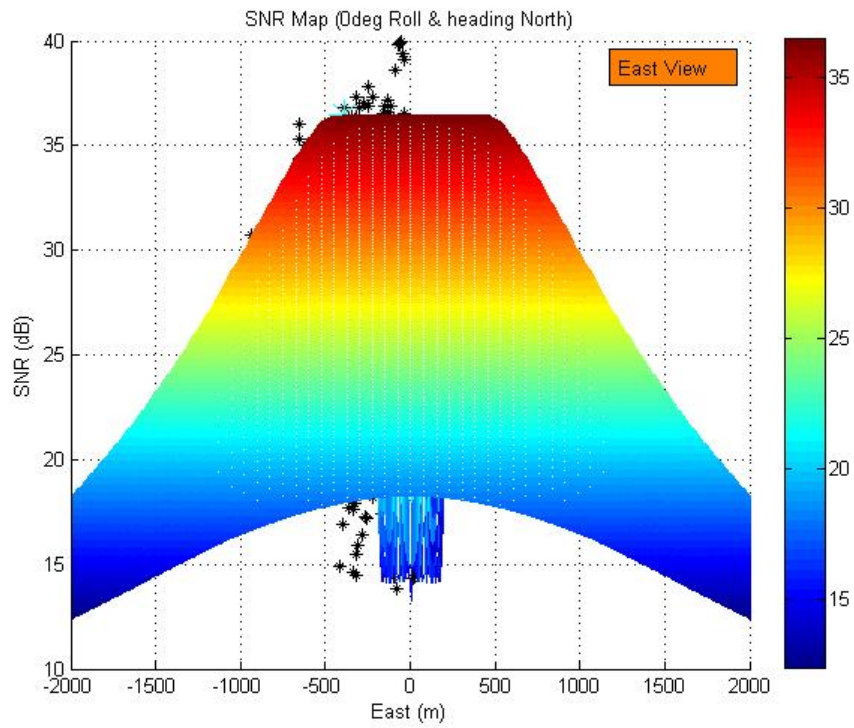


Figure 26. Actual SNR Data Superimposed onto the SNR Map (East View).

THIS PAGE INTENTIONALLY LEFT BLANK

VI. EXTREMUM SEEKING CONTROL

A. BACKGROUND

The Unmanned Systems Lab in NPS has designed a real-time adaptive optimization algorithm which integrates an extremum seeking algorithm with a gradient-based controller to obtain an optimal UAV loitering posture to maximize link quality between one UAV and two transmitting ground nodes. The works from the Unmanned Systems Lab (Refs. [1], [10], and [11]) are briefly discussed in this chapter.

B. HARDWARE-IN-THE-LOOP (HIL) TEST

The primary objective of the HIL simulation test is to verify the autopilot guidance and control algorithm in the laboratory before performing a flight test. The overall structure of the control algorithm is shown in Figure 26.

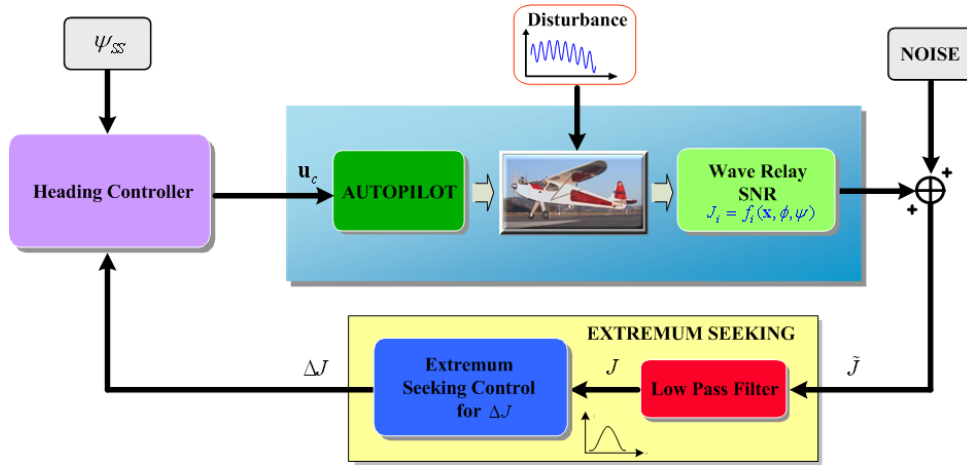


Figure 27. Diagram of Extremum Seeking-based Control Strategy for Autonomous UAV Control [From [10]]

The design allows two transmitting ground nodes to send signals to the UAV. The mathematical SNR model is used to generate the simulated SNR reading between the UAV and the transmitting ground node. The UAV motion is simulated by a Piccolo simulator. The heading command is controlled based on the gradient value obtained from

the extremum seeking loop where a steady-state heading command is used to make the UAV orbit an optimal settling point with a constant radius.

1. HIL Test Set-up

The set-up for the HIL test is as follows:

Ground Transmitting Node

Location of Node 1: 3500 m (east), 114.5 m (north), 5 m (up)

Location of Node 2: -1000 m (east), 614.5 m (north), 5 m (up)

Rascal UAV

Initial location: 10 m (east), 0 m (north), 600 m (up)

Speed: constant at 20 m/s

Altitude: constant at 600m

The set-up for the test is designed in such a way that there is one location that gives the maximum SNR within the intersection area as shown in Figure 27. The maximum SNR point is located in the middle along the intersection lines between the two nodes.

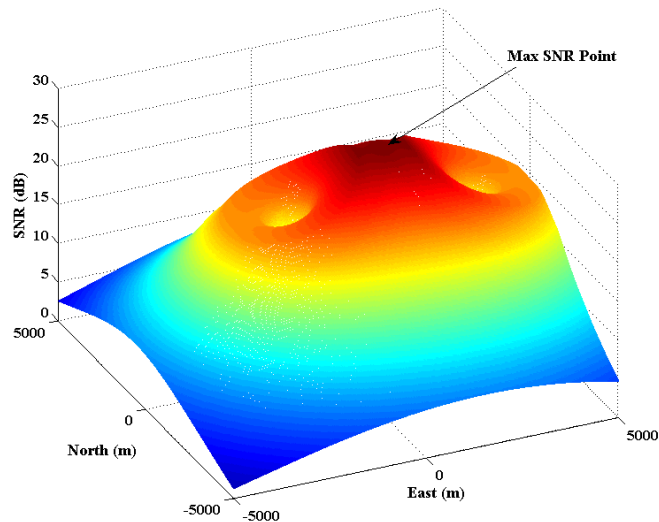


Figure 28. 3D Map of SNR Distribution from Two Antenna Nodes [From [10]]

2. HIL Test Results

Initially, the UAV is located around the origin and starts moving in a circular path to the optimal point between the two nodes (refer to Figure 28). Near the optimal point, the UAV changes from a flying mode to an orbiting mode with a constant radius, following the commands from the steady-state heading rate. As expected, the optimal location lies on the line of the intersection area between the two nodes as shown in Figure 29.

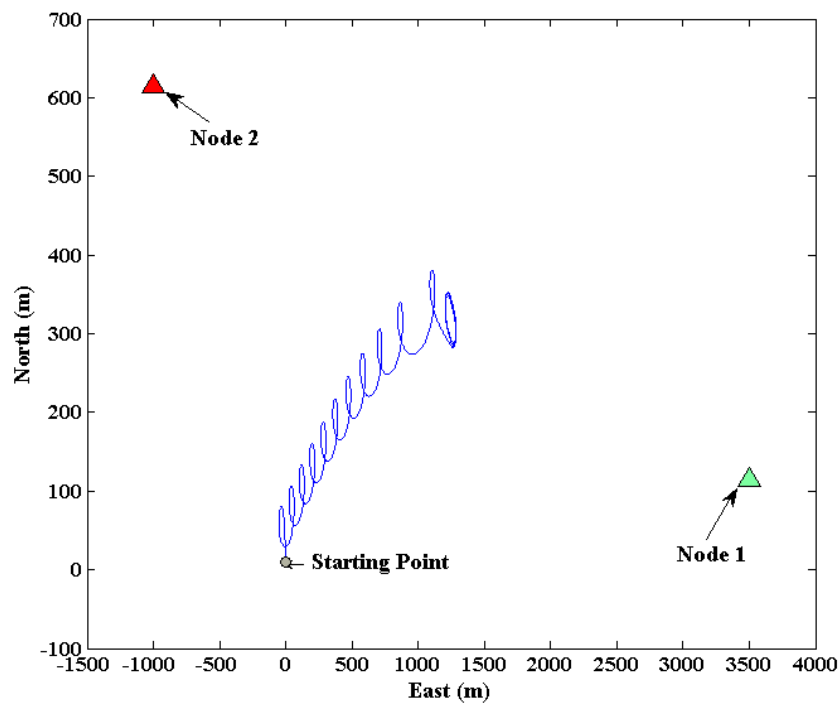


Figure 29. UAV Flight Trajectory with Respect to Two Antenna Nodes Based on Commands from Extremum Seeking Controller [From [10]]

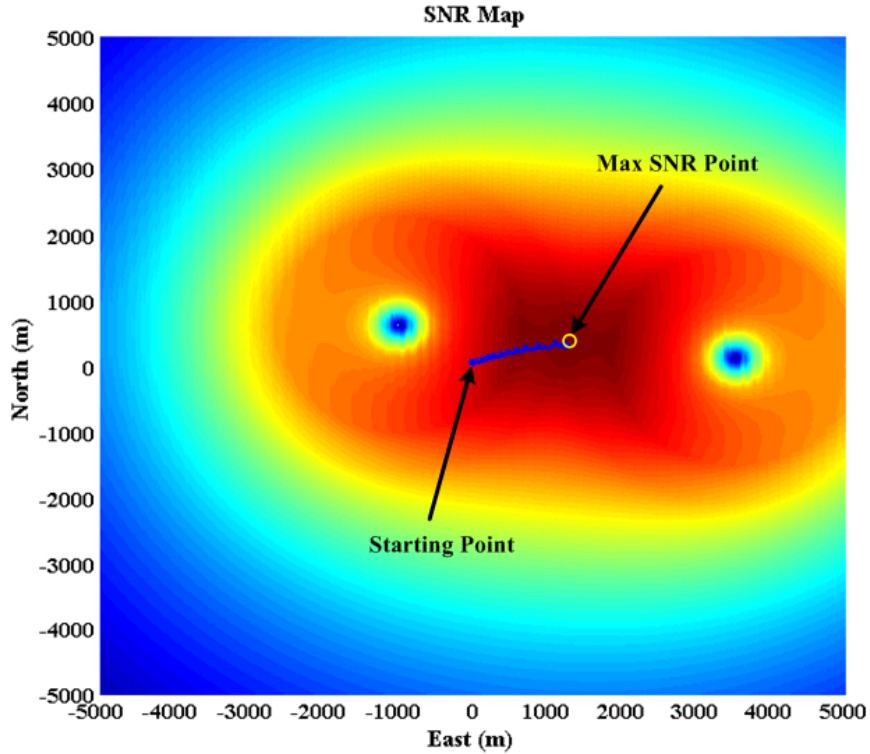


Figure 30. UAV Flight Trajectory Superimposed onto the 2D Projection of the SNR Distribution [From [10]]

Figure 30 and Figure 31 show the SNR variation with time at Nodes 1 and 2 respectively. As expected, SNR increases when the UAV is moving towards Node 1 and decreases when moving away from Node 2. The SNR settles around the optimal point that gives the best possible SNR (~32 dB) between the two nodes.

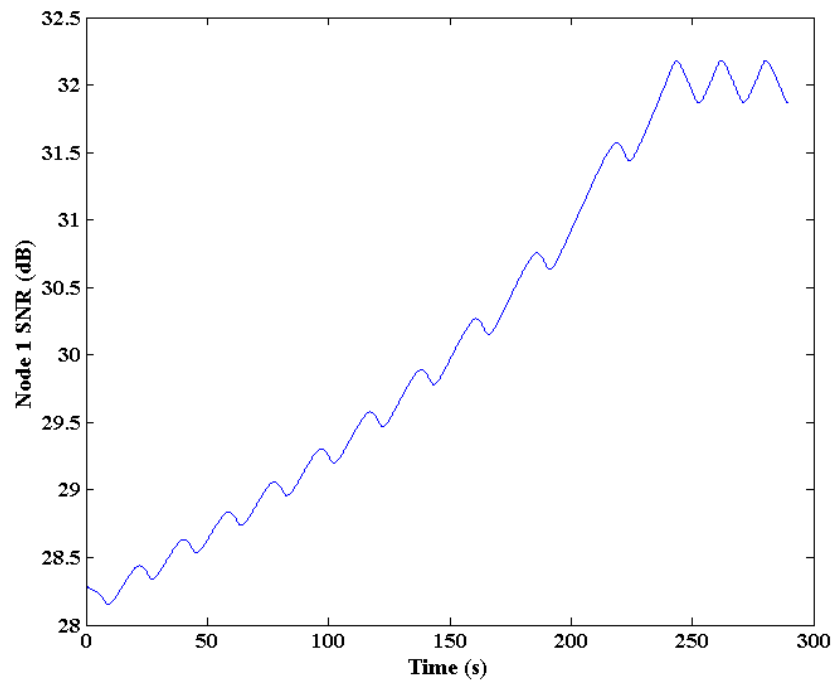


Figure 31. SNR Variation with Time between the UAV and Node 1 [From [10]]

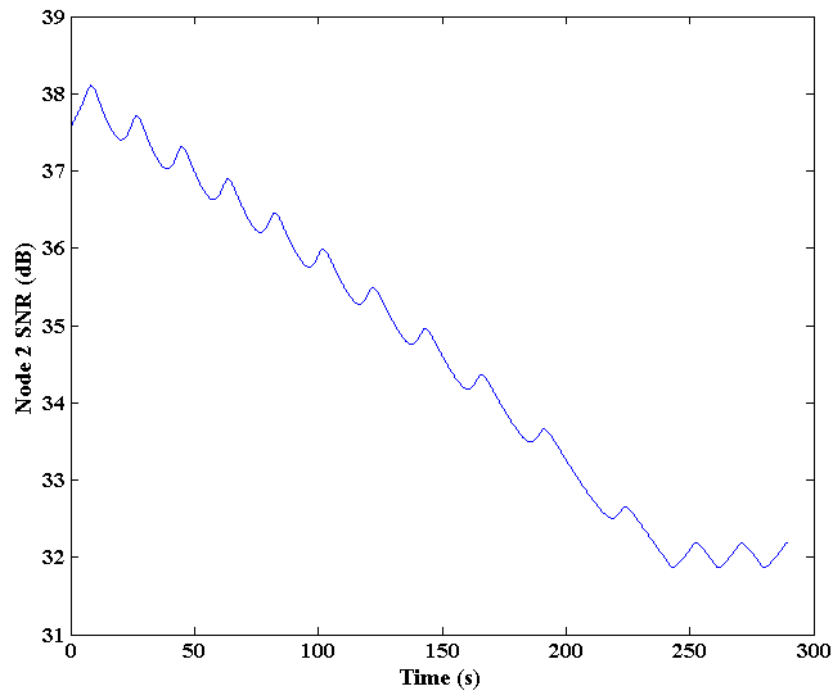


Figure 32. SNR Variation with Time between the UAV and Node 2 [From [10]]

The rate of change of the cost function is shown in Figure 32. It is seen that the rate of the SNR value goes to zero as the UAV reaches the optimal point where the gradient value is zero.

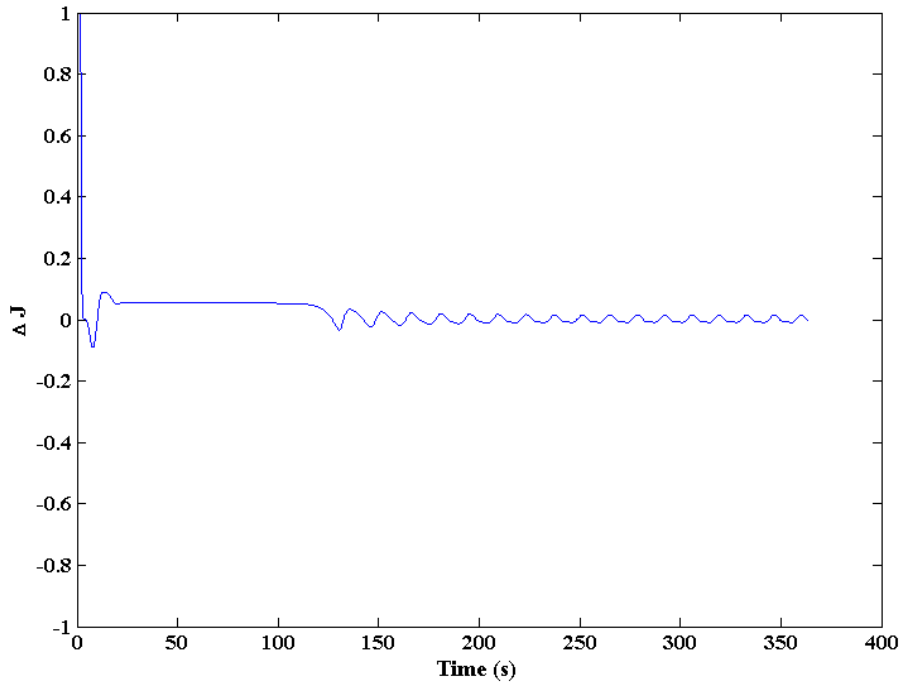


Figure 33. Rate of Change of the Cost Function (SNR) with Time [From [10]]

VII. COMMUNICATION LINKS FLIGHT TEST

A. BACKGROUND

The communication links flight test was conducted as part of the TNT experimentation program (TNT-09-01) at McMillan Air Field in Camp Roberts, California on November 20, 2008. The test was conducted with two stationary ground nodes and the Rascal UAV. The two ground nodes acted as the command station and the survey vehicle while the Rascal UAV functioned as the relay vehicle. The primary objective was to validate the designed onboard adaptive optimization algorithm that would drive the Rascal UAV to an optimal loitering flight path and maximize the SNR between the two nodes and the UAV.

B. SNR DATA ACQUISITION & MANAGEMENT

Currently, the onboard PC-104 computer on the Rascal is unable to extract the SNR value directly from the Wave Relay's management message. As such, the SNR value will need to be extracted on the Linux machine (See Figure 34) located at the ground station and sent to the local host computer prior to transmission to the onboard computer. There is a switch on the local host computer which controls the type of SNR reading sent to the UAV. Currently, the switch caters for the following three types of SNR readings:

1. Model-based SNR. This SNR reading is generated using the mathematical SNR model based on the current position and orientation of the UAV.
2. Real-time SNR. This SNR reading is the actual SNR value computed by the Wave Relay radios.
3. Mixed SNR. This SNR reading is based on the mathematical SNR model modified by the updated actual SNR reading from the Wave Relay radios.

The author intended to test the model-based and the real-time SNR during the flight test but due to lack of airspace time, only the model-based method was successfully carried out.

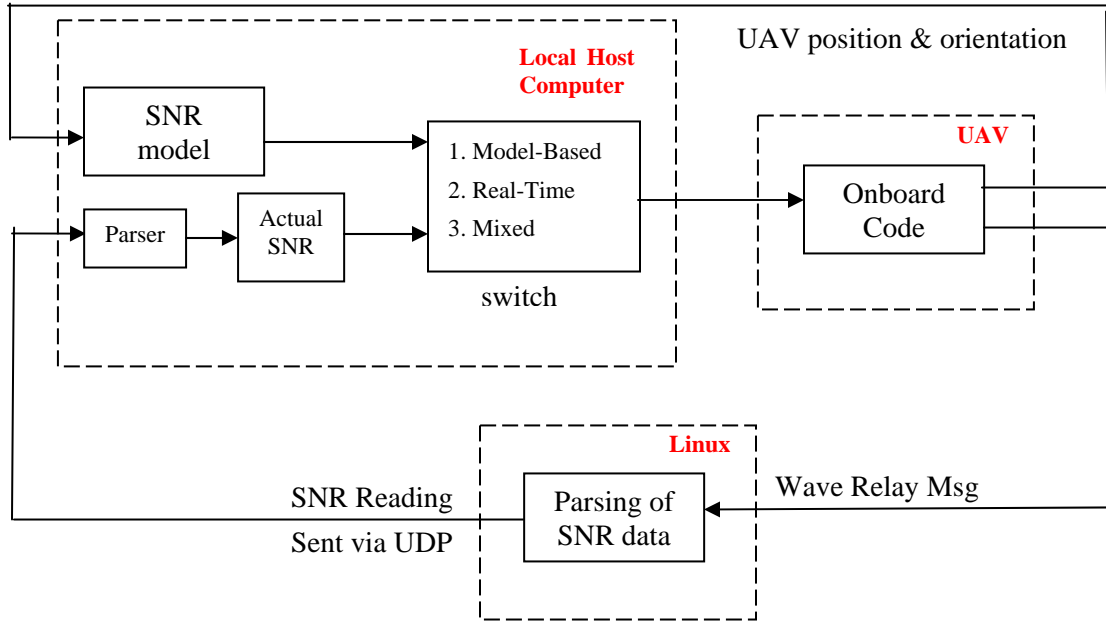


Figure 34. SNR Data Acquisition & Management Structure.

In the setup, there were two ground nodes with the Rascal UAV acting as the relay node between the two nodes. As such, there will be two SNR data values - one from the link between the UAV and the GCS and the other from between the remote node and the UAV. Currently, the combined SNR sent to the onboard computer is computed by taking the average of the two SNR data values.

C. SETUP

The setup for the flight test was as follows:

Ground Control Station (GCS) Node

Antenna: 3 x 9 dB vertically polarized sector antenna (SA24-120-9)

Position: 35.71675 (lat) / -120.76459 (lon) (refer to Figure 35)

Altitude¹: 272m (above mean sea level)

Remote Node

Antenna: 3 x 9 dB vertically polarized sector antenna (SA24-120-9)

Position: 35.73798 (lat) / -120.78639 (lon) (refer to Figure 35)

Altitude¹: 310m (above mean sea level)

The remote was placed such that there was no line-of-sight between the GCS node and the remote node.

Rascal UAV

Antenna: 2.2 dB omni-directional antenna (HG2402RD-RSF)



Figure 35. Relative Location of the GCS node and Remote Node [From Google Earth].

D. FLIGHT TEST RESULTS AND ANALYSIS

1. UAV Flight Trajectory

Figure 36 shows the flight trajectory of the UAV during the test. Initially, the UAV was in a holding pattern orbiting north of the GCS node. When the control algorithm was activated, the UAV started to move in the direction of the steepest increase in the SNR value. When the UAV reached the region of peak SNR, a steady-state heading command was passed to make the UAV orbit around the optimal point. It was observed that the orbit around the optimal point was elongated and not a circular path as predicted by the HIL simulation.

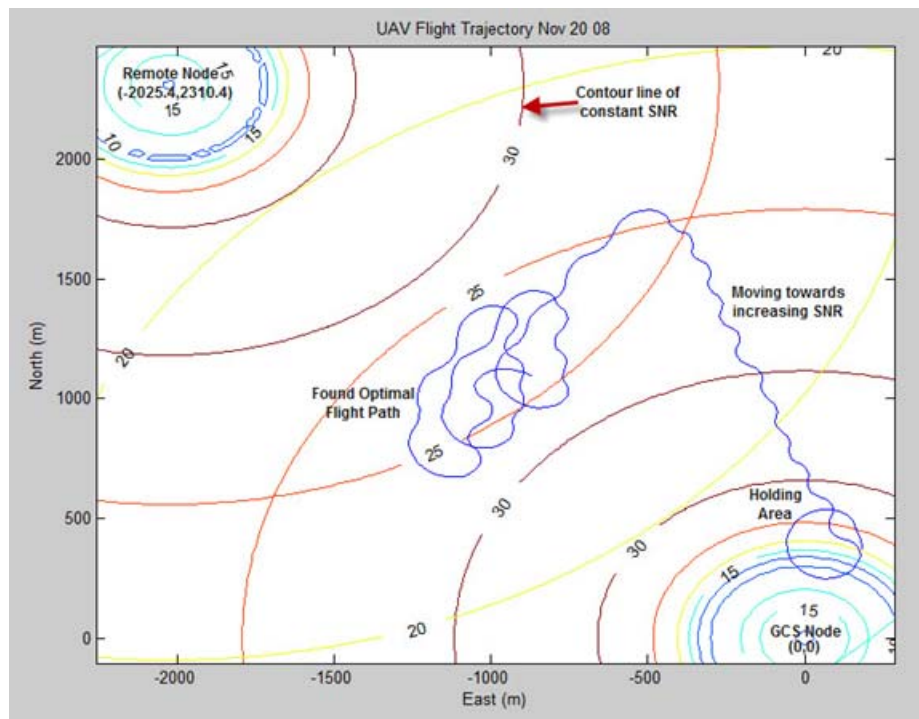


Figure 36. UAV Flight Path during the TNT Experimental Program.

The circular lines shown in Figure 36 are contour lines of constant SNR. The contour lines, generated from the SNR map, show the predicted SNR in east-north coordinates for a stationary (non-dynamic) UAV with fixed altitude, heading, and bank angle.

2. SNR Variation along Flight Trajectory

Figure 37 and Figure 38 show the actual SNR variation with time between the UAV (sender) and GCS node (receiver) and between the remote node (sender) and UAV (receiver) respectively. As expected, the algorithm drove the UAV to fly towards the optimal region that gave the best possible SNR (~23 dB) between the two nodes.

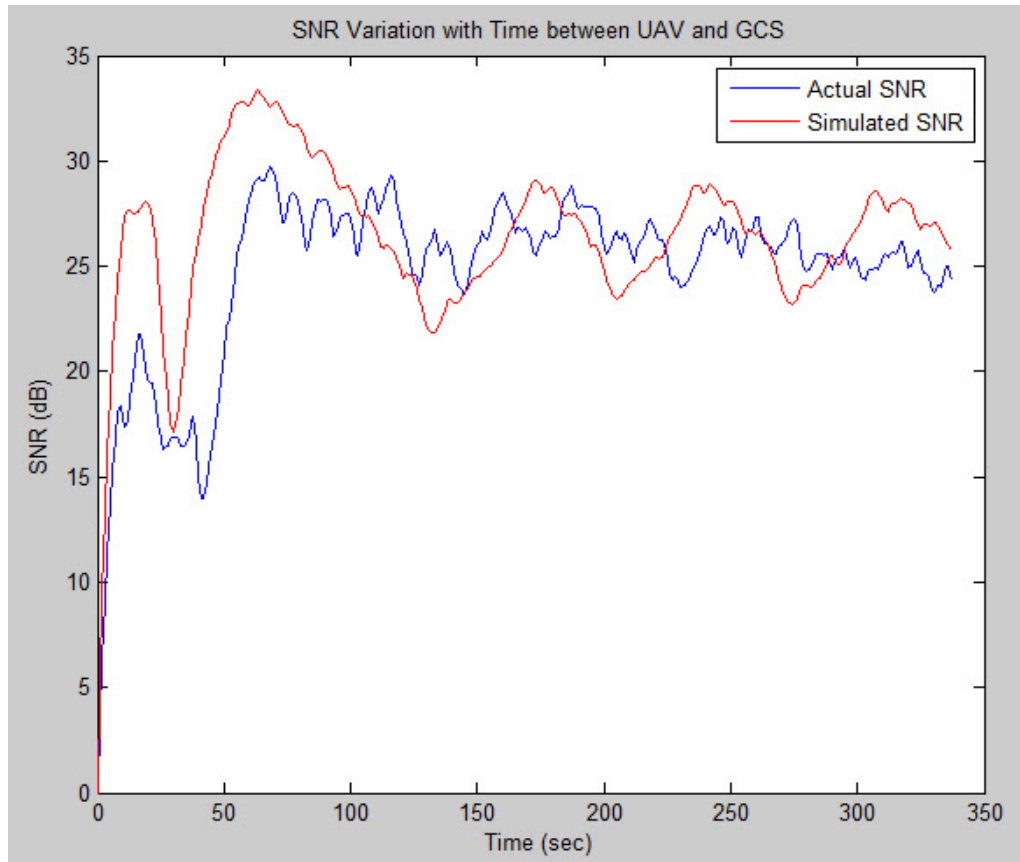


Figure 37. SNR Variation with Time between the UAV (sender) and GCS Node (receiver).

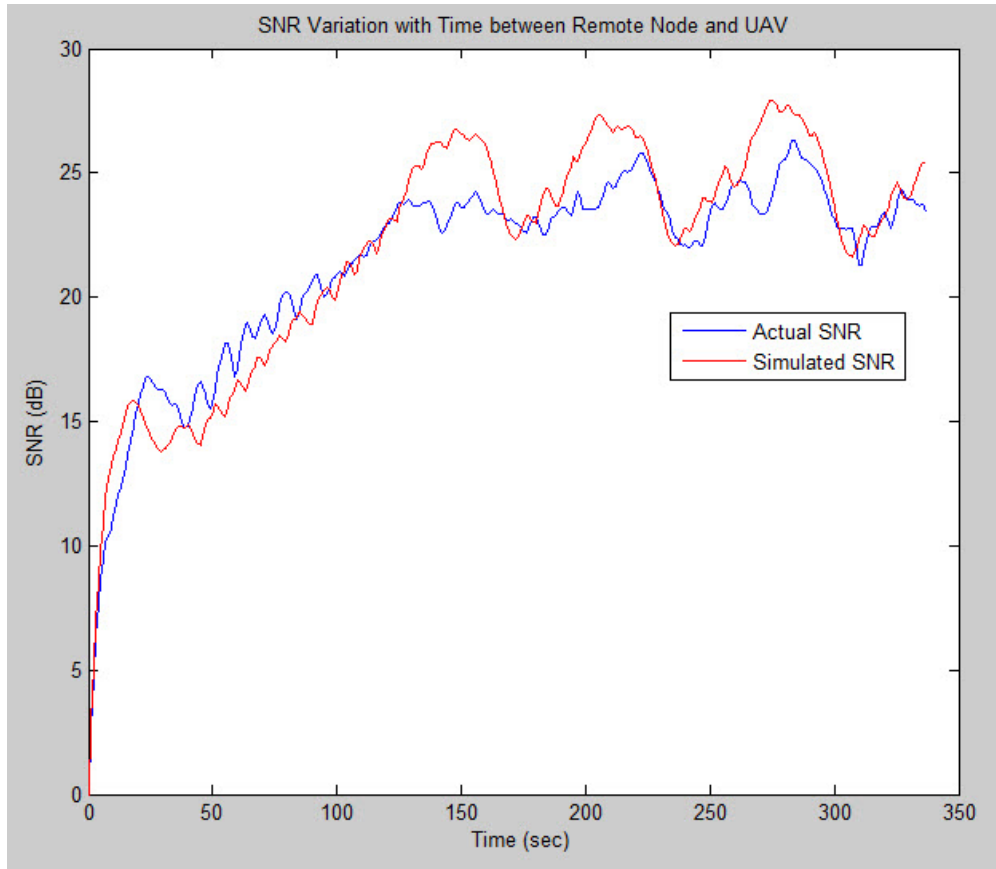


Figure 38. SNR Variation with Time between the Remote Node (sender) and UAV (receiver).

3. Comparison of Actual SNR data with Simulated SNR Data

Figure 39 shows the actual average SNR data from the flight test while Figure 40 shows the simulated average SNR data from the model. It is seen that the SNR for both figures are low at the holding area and move towards a higher value at the optimal region.

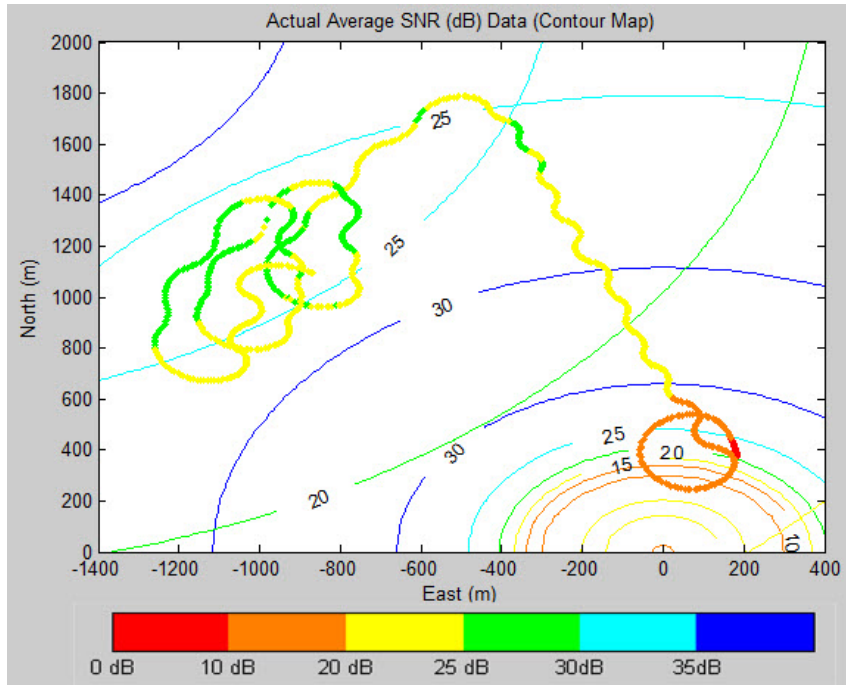


Figure 39. Actual (Measured) Average SNR (dB) along Rascal Flight Trajectory obtained from Flight Test.

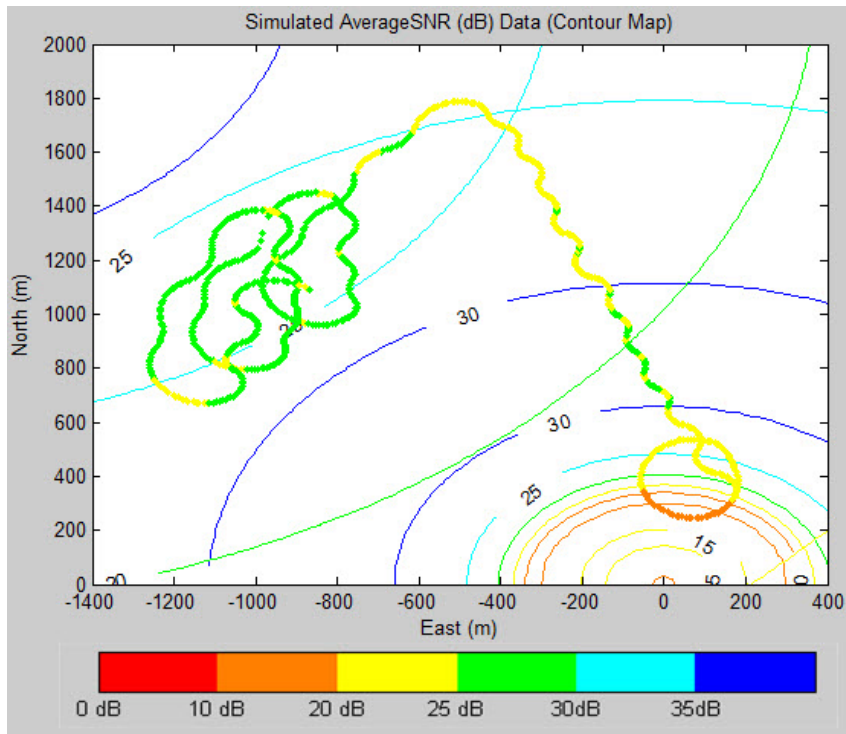


Figure 40. Simulated Average SNR (dB) along Rascal Flight Trajectory obtained from Flight Test.

Figure 41 shows the error between the actual and simulated SNR data. It is seen that the simulated SNR compared nicely with the actual SNR data from the flight test. The error of the simulated model with respect to the actual SNR data was within 15% except for the holding area where the error was more than 30%. The holding area is near the GCS node and the model is not accurate at this near range. Hence, the simulated SNR reading between the GCS and UAV tends to show a large error in the holding area.

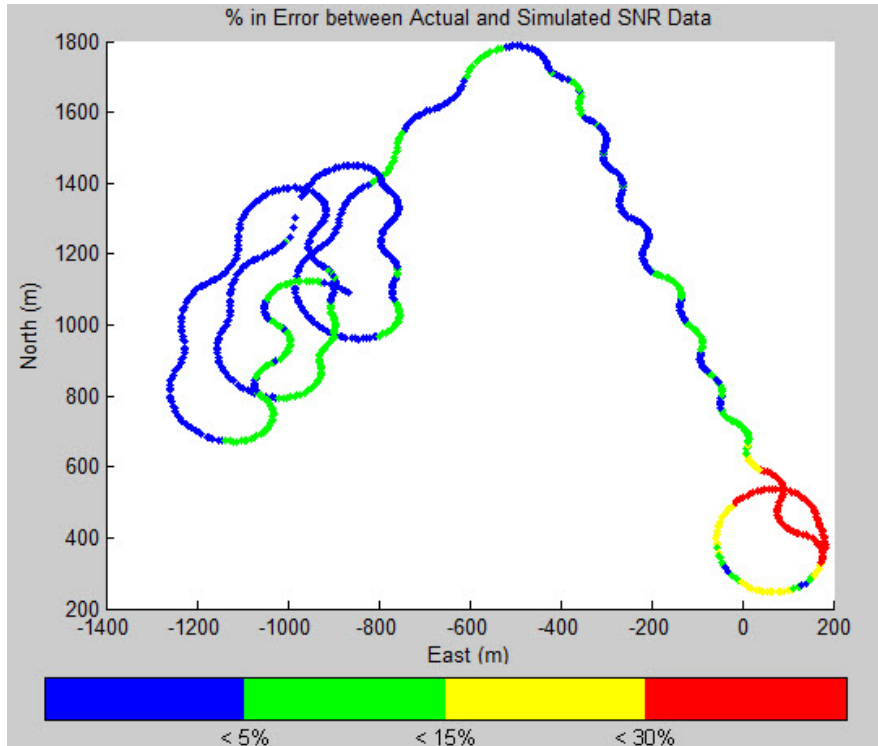


Figure 41. SNR Error (in %) between Simulated Reading and Actual Flight Test Data.

VIII. CONCLUSIONS & FUTURE WORKS

A. CONCLUSIONS

In this thesis, a simple propagation model was developed to predict the link quality (SNR, received power, and link budget) of a communication link between the UAV and ground node. The model was then used to generate simulated SNR “measurements” for the hardware-in-the-loop (HIL) simulation of the extremum-seeking control algorithm. A flight test was carried out with the Rascal UAV on August 1, 2008, and the experiments successfully demonstrated the mathematical model’s ability to compute and predict the SNR for a given communication channel at McMillan Air Field in Camp Roberts, California.

The next step saw the development of autopilot guidance and a control algorithm to drive the UAV to reposition itself autonomously in order to maintain an optimal loitering flight path to achieve the optimal communication link quality between two transmitting ground nodes. The real-time optimization algorithm was based on the extremum-seeking approach with a gradient-based controller. A flight test was carried out on November 20, 2008 and the experiments successfully demonstrated the effectiveness of the extremum-seeking control algorithm for controlling the UAV to the optimal flight path using model-based SNR.

B. FUTURE WORK

In this thesis, the ground nodes were assumed to be stationary to simplify the problem. The next logical goal would be to remove the assumption and extend the SNR model and extremum-seeking control algorithm to accept moving ground nodes.

Others areas that can be explored further include the following:

1. Deployment of multiple UAVs to form an optimized communication chain between the command station and survey vehicles. This will extend the range of the survey vehicles.

2. The use of gliders to replace the UAV as the relay vehicles. The glider (Figure 42) is suggested as the endurance of the glider is longer than a UAV operating in a tactical environment and thus will increase the mission time of the survey vehicle.



Figure 42. Biological Soaring Gliders (NPS)

APPENDIX A. ANTENNA DATASHEETS

Laird
TECHNOLOGIES®

SA24



global solutions :
local support ..

Vertically Polarized Sector Antennas 2400 to 2485 MHz Operation

The vertically polarized sector antenna systems offered by Laird Technologies are constructed of UV stable fiberglass radomes for extremely long service life in the most demanding conditions. The antennas are constructed using corrosion resistant metal elements and a unique air dielectric system which are more stable than PCB based antenna systems because they don't absorb moisture, which can degrade the performance of PCB based antenna systems. The 14dB sectors come with a stainless steel scissor bracket system for ease of installation and alignment. The 9dBi sector comes with a galvanized steel bracket with stainless steel hardware.

Features and Benefits:

- Vertically polarized
- 90 deg, 120 deg and 180deg models with gains from 9dBi to 14dBi
- Type N female integrated connector
- Extremely rugged for long service life in extreme environments
- Weatherproof

Applications

- 2.4 GHz GSM band applications
- 802.11b and 802.11g wireless systems
- WiFi base station antennas
- Point to multi-point Systems
- Wireless Internet

For sales information:
Telephone 801-572-3024
E-Mail sales@pacwireless.com

or visit: www.pacwireless.com

www.pacwireless.com

Specifications

Parameter	Min	Typ	Max	Units
Frequency Range	2400		2485	MHz
Input Return Loss (S11)		-14		dB
VSWR		1.5:1		
Impedance		50		OHM
Input Power			100	W
Pole Diameter (OD)	1" (25)		2" (50)	Inch (mm)
Operating Temperature	-40		+70	Deg C
2400-2485 MHz	SA24-90-9	SA24-120-9	SA24-180-14	
Gain	9.5 dBi	9 dBi	14 dBi	
Horizontal Beam Width†	90 deg	120 deg	180 deg	
Vertical Beam Width		30 deg	10 deg	
Front to Back		25 dB	25 dB	
Mechanical Down tilt	45 deg		10 deg	
Weight		25oz (0.7kg)	11lb (5kg)	
Dimensions (LxWxH)		10" x 6.5" x 2.5" (254 x 165 x 63.5mm)	40" x 10.25 x 7" (1020 x 260 x 180mm)	

Wind Loading				
Model	Sq. In	100MPH	125MPH	100MPH 1/2" radial ice
SA24-90-9	65	16.3 lb	25.4 lb	17 lb
SA24-180-14	400	100 lb	156 lb	102 lb

System Ordering:

SA24-90-9	9dBi 90deg 2.4GHz VPOL sector antenna
SA24-120-9	9dBi 120deg 2.4GHz VPOL sector antenna
SA24-180-14	14dBi 180deg 2.4GHz VPOL sector antenna

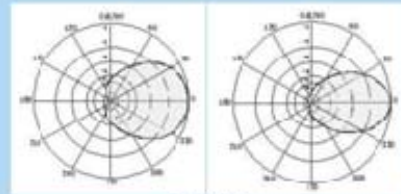
Notes:

- All shipments F.O.B. Schaumburg, IL 60173
- All antennas carry a 2 Year Warranty

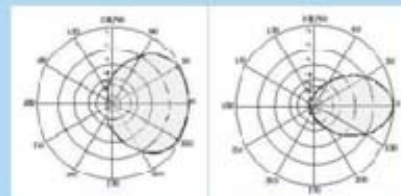
Any information furnished by Laird Technologies and its agents is believed to be accurate and reliable. Responsibility for the use and application of Laird Technologies materials rests with the end user since Laird Technologies and its agents cannot be aware of all potential uses. Laird Technologies makes no warranties as to the fitness, merchantability, or suitability of any Laird Technologies materials or products for any specific or general uses. Laird Technologies shall not be liable for incidental or consequential damages of any kind. All Laird Technologies products are sold pursuant to the Laird Technologies domestic terms and conditions of sale in effect from time to time, a copy of which will be furnished upon request.

Prices/Features subject to change without notice.

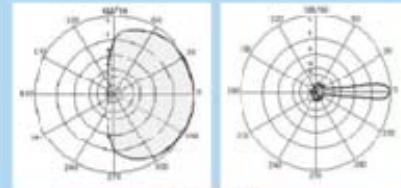
Antenna Patterns



SA24-90-9



SA24-120-9



SA24-180-14



global solutions :
local support™

2.4 GHz 2.2 dBi Reverse Polarity SMA "Rubber Duck" Wireless LAN Antenna

Model: HG2402RD-RSF

Features

- Compact size, only 4.7" long
- Tilt and swivel design
- RP-SMA Connector
- 802.11b, 802.11g and Bluetooth® compatible



Description

This compact 2.4GHz omnidirectional "rubber-duck" WiFi antenna provides broad coverage and 2.2 dBi gain. It is a coaxial sleeve design with an omni-directional pattern. It is ideally suited for IEEE 802.11b and 802.11g wireless LANs, Bluetooth® and other WLAN applications.

Only 4.7" long, this flexible antenna features a tilt-and-swivel reverse-polarity SMA plug connector, allowing them to be used vertically, at a right angle, or any angle in-between. It is suitable as a replacement antenna for many access points and radios that are equipped with reverse-polarity SMA connectors including D-Link®, Linksys® WET11 and others (Note: This RF antenna is used as a "replacement" antenna rather than a "range extender" antenna. It should yield similar range to most radio's stock antennas).

Application Note: This antenna is not for use with U.S.Robotics® RP-SMA equipped devices.

Specifications

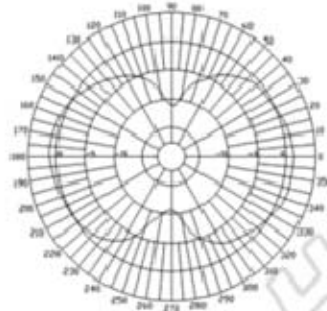
Electrical Specifications

Frequency	2400-2500 MHz
Gain	2.2 dBi
Impedance	50 Ohm
VSWR	< 2.0

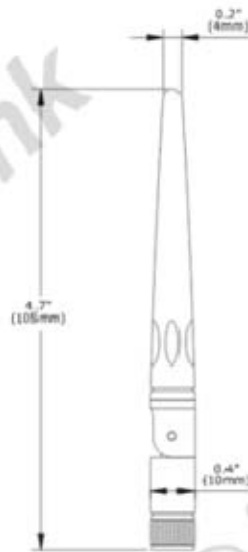
Mechanical Specifications

Weight	0.52 oz. (15 g)
Length	4.7" (105 mm)
Diameter	0.4" (10 mm)
Finish	Matte Black
Connector	Reverse Polarity SMA Plug
Operating Temperature	-40° C to 185° C (-40° F to 185° F)
Polarization	Vertical
RoHS Compliant	Yes

Antenna Gain Pattern



Vertical



LIST OF REFERENCES

- [1] D. J. Lee, K. Kam, I. Kaminer, Kragelund , S. P. and D. P. Horner, "High bandwidth communication links between distributed mobile robots for wireless networking using small UAVs via extremum seeking control," AIAA Unmanned Unlimited Conference, Apr 2009.
- [2] Cheryl Lynn Bauman, "Autonomous Navigation of a Ground Vehicle to Optimize Communication Link Quality," Thesis, Virginia Polytechnic Institute and State University, 2006.
- [3] Cory R. Dixon and Eric W. Frew, "Cooperative Electronic Chaining Using Small Unmanned Aircraft," AIAA 2007 Conference and Exhibit, 2007.
- [4] Kartik B. Ariyur and Miroslav Krstic, "Real-Time Optimization by Extremum-Seeking Control. Wiley-Interscience publication," 2003.
- [5] Miroslav Krstic, "Extremum seeking feedback tools for real-time optimization," Large Scale Robust Optimization, Nov 2005.
- [6] C. E. Shannon, "Communication In The Presence Of Noise," Proceedings of the IEEE, vol. 86, pp. 447-457, 1998.
- [7] T. S. Rappaport, "Wireless Communications : Principles and Practice," 2nd ed. Upper Saddle River, N.J: Prentice Hall PTR, 2002.
- [8] Vladimir N. Dobrokhodov, Oleg A. Yakimenko, Kevin D. Jones, Isaac I. Kaminer, Eugene Bourakov, Ioannis Kitsios and Mariano Lizarraga, "New generation of rapid flight test prototyping system for small unmanned air vehicles," AIAA Modeling and Simulation Technologies Conference and Exhibit, 2007.
- [9] Anonymous Wave relay QUAD radio router. www.persistentsystems.com
- [10] D. J. Lee, K. Kam, I. Kaminer, "High bandwidth communications links using small UAV via extremum seeking control," NPS Internal Report, 2008.

- [11] D. J. Lee, I. Kaminer, V. Dobrokhodov and K. D. Jones, "Feature following and distributed navigation systems development for a small unmanned aerial vehicle with low-cost sensors," AIAA Guidance, Navigation, and Control Conference, Aug 2008.

INITIAL DISTRIBUTION LIST

1. Defense Technical Information Center
Ft. Belvoir, Virginia
2. Dudley Knox Library
Naval Postgraduate School
Monterey, California
3. Professor Isaac I. Kaminer
Naval Postgraduate School
Monterey, California
4. Dr Deok Jin Lee
Naval Postgraduate School
Monterey, California
5. Professor Knox T. Millsaps
Chairman, Department of Mechanical and Astronautical
Naval Postgraduate School
Monterey, California
6. Professor Yeo Tat Soon
Director
Temasek Defence Systems Institute
National University of Singapore
Singapore
7. Tan Lai Poh (Ms)
Assistant Manager
Temasek Defence Systems Institute
National University of Singapore
Singapore